

# Dynamical density functional theory: binary phase-separating colloidal fluid in a cavity

A J Archer<sup>‡</sup>

H H Wills Physics Laboratory, University of Bristol, Bristol BS8 1TL, UK

**Abstract.** The dynamical density functional theory of Marconi and Tarazona [*J. Chem. Phys.*, **110**, 8032 (1999)], a theory for the non-equilibrium dynamics of the one-body density profile of a colloidal fluid, is applied to a binary fluid mixture of repulsive Gaussian particles confined in a spherical cavity of variable size. For this model fluid there exists an extremely simple Helmholtz free energy functional that provides a remarkably accurate description of the equilibrium fluid properties. We therefore use this functional to test the assumptions implicit in the dynamical density functional theory, rather than any approximations involved in constructing the free energy functional. We find very good agreement between the theory and Brownian dynamics simulations, focusing on cases where the confined fluid exhibits phase separation in the cavity. We also present an instructive derivation of the Smoluchowski equation (from which one is able to derive the dynamical density functional theory) starting from the Liouville equation – a fully microscopic treatment of the colloid *and* solvent particles. This ‘coarse-graining’ is, of course, not exact and thus the derivation demonstrates the physical assumptions implicit in the Smoluchowski equation and therefore also in the dynamical density functional theory.

## 1. Introduction

For a multi-component fluid composed of particles with a large size difference between the different components, a theoretical description of the (inhomogeneous) fluid dynamics is challenging due to the varying equilibration timescales for the different species of particles in the fluid. Colloidal suspensions are a particular example of such complex fluids. Typically, the colloids are 10–1000nm in diameter, whereas the solvent molecules are, in the case of water,  $\sim 0.2$ nm. The situations in which a theory could be used to describe the motion of inhomogeneous (confined) colloidal particles are many. For example, in colloidal physics the use of optical tweezers to confine and then move individual or groups of colloids is common [1]. Simulating such a fluid is also computationally expensive, because of the huge numbers of solvent molecules required when simulating even a limited number of colloids. A common approach to such systems is to integrate out the degrees of freedom of the smaller particles in order to render a

<sup>‡</sup> andrew.archer@bristol.ac.uk

description of the system based only on the (much smaller) phase space corresponding to the degrees of freedom of the big colloid particles [2].

In the case of colloidal fluids in thermal (static) equilibrium, this ‘coarse-grained’ approach is, at least formally, well understood and one is able to formulate an effective Hamiltonian for the fluid involving only the phase space coordinates of the big particles. Of course, the effective potential between the big particles is, in general, many-body in character and dependent on the density of both the solvent and colloid particles [2, 3]. For example, the depletion potential, or effective solvent mediated interaction potential, between big hard-sphere particles dissolved in a solvent of small hard spheres, is oscillatory for large separations [4] and is therefore very different from the ‘bare’ potentials one typically encounters between the particles of a molecular fluid. However, for the non-equilibrium dynamics of colloidal fluids, coarse-graining is carried out on a more ad-hoc basis. A common approach is to use the effective solvent mediated potential obtained from the equilibrium theory together with stochastic equations of motion – i.e. the force on the colloids due to collisions with the solvent particles is modelled as a random white noise term and a frictional (Stokes) one-body drag force. The colloids are thus modelled as Brownian particles. From the (Langevin) equations of motion for the Brownian particles one can obtain the Fokker-Planck (Smoluchowski) equation [5] for the colloid probability distribution function in phase space, and thus one is able to determine non-equilibrium dynamic properties of the colloidal fluid. In going to such a stochastic description of the dynamics one inevitably neglects hydrodynamic effects. We justify the above stochastic approach in Sec. 4.

In this paper we consider cases of a model colloidal fluid confined in time dependent one-body external potentials. We focus on the time dependence of the fluid one-body density profile, using the dynamical density functional theory (DDFT) derived recently by Marconi and Tarazona [6, 7] §. In a recent paper [9] (see also Ref. [10]), it was demonstrated that this DDFT could be derived from the Smoluchowski equation, by making the assumption that the form of correlations between particles in an inhomogeneous fluid out of equilibrium, is the same as in an equilibrium fluid with the same one body density profile [6, 7, 9]. We apply the DDFT to the dynamics of a particular model colloidal fluid, the binary Gaussian core model (GCM), making a comparison between the results from the DDFT and Brownian dynamics (BD) simulation results. Dzubiella and Likos [11] made a similar comparison for the one component GCM, and found good agreement between theory and simulations. The GCM is a simple model for the effective potential between the centers of mass of polymers or dendrimers in solution [3, 12, 13, 14, 15, 16, 17, 18]. The reason Dzubiella and Likos chose this particular model fluid is that there exists a very simple, yet remarkably accurate (as we demonstrate below for mixtures) Helmholtz free energy functional for describing the equilibrium properties of the GCM [3, 19, 20, 21, 22, 23, 24] and thus by using this functional combined with the DDFT they were able to test some of the

§ The key DDFT equation (Eq. (16)) was proposed originally, without derivation, by Evans [8].

approximations inherent in the DDFT, rather than the approximations involved in the free energy functional. The DDFT has also been successfully applied to situations with steady currents [25, 26] and very recently, Rex *et al* have applied the DDFT to the GCM fluid in shear and travelling wave potentials [27]. For these cases they also find good agreement between theory and simulations. One particular question we wish to address here is whether the DDFT can incorporate dynamical effects that are specific to colloidal fluids composed of two different species of colloids and, in particular, dynamical effects arising when there is phase separation and wetting phenomena in a confined colloidal fluid.

The paper is arranged as follows: In Sec. 2 we introduce and briefly describe the DDFT. The results from the application of the DDFT are presented in Sec. 3. In Sec. 4 we give an alternative derivation of the Smoluchowski equation. Starting from the Liouville equations for a mixture of colloid and solvent particles, we first obtain the Kramers equation and then from this the Smoluchowski equation. These equations can also be derived as the (generalised) Fokker-Planck equations for a system of Brownian particles with stochastic equations of motion. The present derivation elucidates some of the physical assumptions concerning the fluid dynamics that are implicit in the Kramers and the Smoluchowski equations. We believe this derivation sheds light on the status of the DDFT and the approximations inherent in this theory. Finally, in Sec. 5 we discuss our results and draw some conclusions.

## 2. The DDFT

Before introducing the DDFT, we recall briefly some of the basic results from *equilibrium* density functional theory (EDFT) [8, 28] that are required for our discussion of the DDFT. The key quantity in EDFT is the Helmholtz free energy functional:

$$F[\rho(\mathbf{r})] = F_{id}[\rho(\mathbf{r})] + F_{ex}[\rho(\mathbf{r})] + \int d\mathbf{r} u_{ext}(\mathbf{r})\rho(\mathbf{r}), \quad (1)$$

which is a functional of  $\rho(\mathbf{r})$ , the fluid one-body density. For simplicity we consider a one-component fluid.  $u_{ext}(\mathbf{r})$  is a one body external potential and

$$F_{id}[\rho(\mathbf{r})] = k_B T \int d\mathbf{r} \rho(\mathbf{r}) [\ln(\Lambda^3 \rho(\mathbf{r})) - 1], \quad (2)$$

is the (exact) ideal gas free energy;  $\Lambda$  is the thermal de Broglie wavelength of the particles.  $F_{ex}[\rho(\mathbf{r})]$  is the excess (over ideal) contribution to the free energy due to interactions between the particles [8, 28]. In EDFT one considers the following grand potential functional

$$\Omega[\rho(\mathbf{r})] = F[\rho(\mathbf{r})] - \mu \int d\mathbf{r} \rho(\mathbf{r}), \quad (3)$$

where  $\mu$  is the chemical potential. The equilibrium density distribution is given by the minimisation condition [8, 28]:

$$\frac{\delta \Omega}{\delta \rho(\mathbf{r})} = 0. \quad (4)$$

Thus, using Eqs. (1) – (4), one obtains the following Euler-Lagrange equation for the equilibrium fluid density profile:

$$0 = k_B T \ln \Lambda^3 \rho(\mathbf{r}) - k_B T c^{(1)}(\mathbf{r}) + u_{ext}(\mathbf{r}) - \mu, \quad (5)$$

where the one body direct correlation function:

$$c^{(1)}(\mathbf{r}) \equiv -\beta \frac{\delta F_{ex}[\rho(\mathbf{r})]}{\delta \rho(\mathbf{r})}. \quad (6)$$

$\beta = 1/k_B T$  is the inverse temperature and  $-k_B T c^{(1)}(\mathbf{r})$  is an effective one body potential that incorporates the effect of the interparticle interactions in the fluid. The central task in EDFT is to find a suitable approximation for  $F_{ex}[\rho(\mathbf{r})]$  for the fluid of interest.  $F_{ex}[\rho(\mathbf{r})]$  is, in general, an unknown quantity. A second functional derivative of  $F_{ex}[\rho(\mathbf{r})]$  gives the inhomogeneous (Ornstein-Zernike) pair direct correlation function:

$$c^{(2)}(\mathbf{r}, \mathbf{r}') \equiv -\beta \frac{\delta^2 F_{ex}[\rho(\mathbf{r})]}{\delta \rho(\mathbf{r}) \delta \rho(\mathbf{r}')}. \quad (7)$$

Often, approximations for  $F_{ex}[\rho(\mathbf{r})]$  are constructed by requiring that the approximate excess Helmholtz free energy functional generate, via Eq. (7), reliable results for  $c^{(2)}(r)$ , the *bulk* pair direct correlation function, about which much is known from the theory of bulk equilibrium fluids [28, 29].

We now move on to consider a non-equilibrium fluid of  $N$  Brownian colloid particles. We denote the position of the  $i^{\text{th}}$  colloid particle by  $\mathbf{r}_i$ , and the set of all position coordinates by  $\mathbf{r}^N \equiv \{\mathbf{r}_1, \dots, \mathbf{r}_N\}$ . The total colloid potential energy  $U_N(\mathbf{r}^N, t)$  is assumed to be of the following form:

$$U_N(\mathbf{r}^N, t) = \sum_{i=1}^N u_{ext}(\mathbf{r}_i, t) + \frac{1}{2} \sum_{j \neq i} \sum_{i=1}^N u_2(\mathbf{r}_i, \mathbf{r}_j) + \frac{1}{6} \sum_{k \neq j \neq i} \sum_{j \neq i} \sum_{i=1}^N u_3(\mathbf{r}_i, \mathbf{r}_j, \mathbf{r}_k) + \dots, \quad (8)$$

which is made up of a one-body term, i.e. a *time-dependent* one-body external potential  $u_{ext}(\mathbf{r}_i, t)$  acts on each fluid particle; a two-body term, which is a sum of (time independent) pair potentials  $u_2(\mathbf{r}_i, \mathbf{r}_j)$ ; a three body term, given by a sum of three-body potentials  $u_3(\mathbf{r}_i, \mathbf{r}_j, \mathbf{r}_k)$  and higher body terms, each given by a sum of multi-body potentials. Since we do not include explicitly the solvent particles, this potential must include contributions from solvent mediated interactions between the colloids as well as the direct (bare) interactions between the colloids – we will return to this issue in Sec. 4||. On the Brownian time scale the equations of motion of the colloids obey the following stochastic (Langevin) equations of motion [30]:

$$\Gamma^{-1} \frac{d\mathbf{r}_i(t)}{dt} = -\frac{\partial U_N(\mathbf{r}^N, t)}{\partial \mathbf{r}_i} + \mathbf{G}_i(t), \quad (9)$$

|| For the purposes of calculating equilibrium fluid properties, all solvent effects are included in the effective potential  $U_N(\mathbf{r}^N, t)$ . However, for *dynamics*, the solvent friction has to be explicitly taken into account.

where  $\Gamma^{-1}$  is a friction constant characterising the one-body drag of the solvent on the colloidal particles and  $\mathbf{G}_i(t) = (\xi_i^x(t), \xi_i^y(t), \xi_i^z(t))$  is a white noise term with the property

$$\begin{aligned} \langle \xi_i^\alpha(t) \rangle &= 0, \\ \langle \xi_i^\alpha(t) \xi_i^\nu(t') \rangle &= 2k_B T \delta_{ij} \delta^{\alpha\nu} \delta(t - t'). \end{aligned} \quad (10)$$

The stochastic equations of motion (9), of course, neglect hydrodynamic interactions between the colloids.

We can define a probability density function  $P^{(N)}(\mathbf{r}^N, t)$  for the  $N$  colloids. The time evolution of  $P^{(N)}(\mathbf{r}^N, t)$  is described by the Smoluchowski equation [5]:

$$\frac{\partial P^{(N)}}{\partial t} = \Gamma \sum_{i=1}^N \frac{\partial}{\partial \mathbf{r}_i} \cdot \left( k_B T \frac{\partial P^{(N)}}{\partial \mathbf{r}_i} + \frac{\partial U_N}{\partial \mathbf{r}_i} P^{(N)} \right). \quad (11)$$

This equation is the (generalised) Fokker-Planck equation for the Langevin equations (9). The Smoluchowski equation is generally presented from this stochastic viewpoint. However, as we show below in Sec. 4, one can argue for its use as an approximation to the exact Liouville equations: By going to the Smoluchowski equation the description of the fluid is reduced to one based solely on the position coordinates of the colloids, rather than utilising the full set of phase space coordinates for the colloid and solvent particles. However, in practice a further reduction is required in order to be able to determine explicitly the dynamics of the colloids. In particular, we focus on the colloid one-body density [9, 10, 29]:

$$\rho(\mathbf{r}_1, t) = N \int d\mathbf{r}_2 \dots \int d\mathbf{r}_N P^{(N)}(\mathbf{r}^N, t). \quad (12)$$

Similarly, the  $n$ -particle density is

$$\rho^{(n)}(\mathbf{r}^n, t) = \frac{N!}{(N-n)!} \int d\mathbf{r}_{n+1} \dots \int d\mathbf{r}_N P^{(N)}(\mathbf{r}^N, t). \quad (13)$$

We now follow closely the derivation in Ref. [9]: Using Eqs. (8), (12) and (13), we find that on integrating Eq. (11), one obtains [9, 31]:

$$\begin{aligned} \Gamma^{-1} \frac{\partial \rho(\mathbf{r}_1, t)}{\partial t} &= k_B T \frac{\partial^2 \rho(\mathbf{r}_1, t)}{\partial \mathbf{r}_1^2} + \frac{\partial}{\partial \mathbf{r}_1} \cdot \left[ \rho(\mathbf{r}_1, t) \frac{\partial u_{ext}(\mathbf{r}_1, t)}{\partial \mathbf{r}_1} \right] \\ &+ \frac{\partial}{\partial \mathbf{r}_1} \cdot \int d\mathbf{r}_2 \rho^{(2)}(\mathbf{r}_1, \mathbf{r}_2, t) \frac{\partial u_2(\mathbf{r}_1, \mathbf{r}_2)}{\partial \mathbf{r}_1} \\ &+ \frac{\partial}{\partial \mathbf{r}_1} \cdot \int d\mathbf{r}_2 \int d\mathbf{r}_3 \rho^{(3)}(\mathbf{r}_1, \mathbf{r}_2, \mathbf{r}_3, t) \frac{\partial u_3(\mathbf{r}_1, \mathbf{r}_2, \mathbf{r}_3)}{\partial \mathbf{r}_1} + \dots \end{aligned} \quad (14)$$

At equilibrium, when  $\partial \rho(\mathbf{r}, t) / \partial t = 0$ , this equation is just the gradient of the (exact) first equation of the YBG hierarchy [29].

We are now in a position to make contact with EDFT. For an *equilibrium* fluid the gradient of  $-k_B T c^{(1)}(\mathbf{r})$  (see Eq. (6)), a one body force due to interactions between particles in the fluid, is given by the following sum-rule [8, 9, 32]:

$$-k_B T \rho(\mathbf{r}_1) \frac{\partial c^{(1)}(\mathbf{r}_1)}{\partial \mathbf{r}_1} = \sum_{n=2}^{\infty} \int d\mathbf{r}_2 \dots \int d\mathbf{r}_n \rho^{(n)}(\mathbf{r}^n) \frac{\partial u_n(\mathbf{r}^n)}{\partial \mathbf{r}_1}. \quad (15)$$

If we assume that we can use (15) for a non-equilibrium fluid we are assuming that the effective one body force on a particle in the fluid due to interactions with the other particles is the same as that in the equilibrium fluid with the *same* one body density profile. We make this assumption and using Eqs. (15) and (1) together with Eq. (14) we obtain the key DDFT equation [6, 7, 9]:

$$\frac{\partial \rho(\mathbf{r}, t)}{\partial t} = \Gamma \frac{\partial}{\partial \mathbf{r}} \cdot \left[ \rho(\mathbf{r}, t) \frac{\partial}{\partial \mathbf{r}} \left( \frac{\delta F[\rho(\mathbf{r}, t)]}{\delta \rho(\mathbf{r}, t)} \right) \right], \quad (16)$$

where  $F[\rho(\mathbf{r}, t)]$  is given by Eq. (1) with  $\rho(\mathbf{r})$  replaced by the time dependent one-body density  $\rho(\mathbf{r}, t)$ . Before commenting on the status of Eq. (16), we note that the above arguments can easily be generalised to the case where there are several different species of colloids. If there are  $Q$  different species of colloids, with  $N_q$  colloids of species  $q$ , such that the total number of colloidal particles is  $N = \sum_{q=1}^Q N_q$ , and the total colloid effective potential energy is (c.f. Eq. (8)):

$$U_N(\mathbf{r}^N, t) = \sum_{q=1}^Q \sum_{i=1}^{N_q} u_{ext}^q(\mathbf{r}_{q,i}, t) + \frac{1}{2} \sum_{q,q'=1}^Q \sum_{j \neq i} \sum_{i=1}^{N_q} u_2^{q,q'}(\mathbf{r}_{q,i}, \mathbf{r}_{q',j}) + \dots \quad (17)$$

In this case, the Smoluchowski equation (11) simply becomes

$$\frac{\partial P^{(N)}}{\partial t} = \sum_{q=1}^Q \Gamma_q \sum_{i=1}^{N_q} \frac{\partial}{\partial \mathbf{r}_{q,i}} \cdot \left( k_B T \frac{\partial P^{(N)}}{\partial \mathbf{r}_{q,i}} + \frac{\partial U_N}{\partial \mathbf{r}_{q,i}} P^{(N)} \right), \quad (18)$$

where  $\Gamma_q^{-1}$  is the friction constant for the  $q^{\text{th}}$  species of colloid particle. One can then integrate Eq. (18) to obtain a DDFT for the one-body density profiles. The one-body density of species  $q$  is:

$$\rho_q(\mathbf{r}_{q,1}, t) = N_q \prod_{i=2}^{N_q} \int d\mathbf{r}_{q,i} \prod_{q' \neq q} \int d\mathbf{r}^{N_{q'}} P^{(N)}(\mathbf{r}^N, t), \quad (19)$$

i.e.,  $\rho_q(\mathbf{r}_{q,1}, t)$  is given by the integral over  $P^{(N)}$  with respect to all the colloid position coordinates other than those of the  $i = 1$  colloid of species  $q$ . The multi-component generalisation of the DDFT equation (16) then becomes:

$$\frac{\partial \rho_q(\mathbf{r}, t)}{\partial t} = \Gamma_q \frac{\partial}{\partial \mathbf{r}} \cdot \left[ \rho_q(\mathbf{r}, t) \frac{\partial}{\partial \mathbf{r}} \left( \frac{\delta F[\{\rho_q(\mathbf{r}, t)\}]}{\delta \rho_q(\mathbf{r}, t)} \right) \right], \quad (20)$$

where the Helmholtz free energy functional for the multi-component colloidal fluid is (c.f. Eq. (1)):

$$\begin{aligned} F[\{\rho_q(\mathbf{r}, t)\}] &= \sum_{q=1}^Q k_B T \int d\mathbf{r} \rho_q(\mathbf{r}, t) [\ln(\Lambda_q^3 \rho_q(\mathbf{r}, t)) - 1] + F_{ext}[\{\rho_q(\mathbf{r}, t)\}] \\ &+ \sum_{q=1}^Q \int d\mathbf{r} u_{ext}^q(\mathbf{r}, t) \rho_q(\mathbf{r}, t). \end{aligned} \quad (21)$$

For an inhomogeneous equilibrium fluid Eqs. (3) and (4) imply that the chemical potential  $\mu = \delta F / \delta \rho(\mathbf{r})$  is a constant throughout the body of the fluid. Similarly, for

an inhomogeneous equilibrium multi-component fluid, the chemical potentials for the different species,

$$\mu_q = \frac{\delta F[\{\rho_q(\mathbf{r})\}]}{\delta \rho_q(\mathbf{r})}, \quad (22)$$

take a constant value throughout the fluid. The DDFT (20) is equivalent to assuming that in the non-equilibrium fluid, this is not the case, and that the gradients of the chemical potentials are the thermodynamic forces driving particle currents  $\mathbf{j}_q$  of each species [9, 8]:

$$\mathbf{j}_q(\mathbf{r}, t) = -\Gamma_q \rho_q(\mathbf{r}, t) \frac{\partial \mu_q}{\partial \mathbf{r}}. \quad (23)$$

On combining this result with the continuity equation

$$\frac{\partial \rho_q(\mathbf{r}, t)}{\partial t} = -\frac{\partial}{\partial \mathbf{r}} \cdot \mathbf{j}_q(\mathbf{r}, t), \quad (24)$$

one obtains the DDFT Eq. (20). The DDFT is clearly not a theory for a colloidal fluid in which there is a temperature gradient. In order to incorporate such an effect in a microscopic theory, one would need to construct an external potential that couples to both the position *and* momentum degrees of freedom of the colloids. In reality, such thermal effects normally also influence the solvent particles. In the present description we have effectively assumed that the solvent acts as a heat bath, keeping the temperature of the colloids at a constant value – even in cases where the change in the external potential is such that one would find an increase in the temperature of the fluid were it a simple (molecular, non-colloidal) fluid – for example under rapid compression.

As we have already mentioned,  $F_{ex}[\{\rho_q(\mathbf{r})\}]$ , the equilibrium excess Helmholtz free energy functional for the fluid mixture is, in principle, an unknown quantity. There exist, depending on the fluid in question, a number of accurate approximate functionals, which give extremely good results for equilibrium fluid density profiles for a wide variety of external potentials (see, for example, Ref. [28] and references therein). This means that the DDFT (20) is a very appealing theory for the dynamics of an *inhomogeneous* colloidal fluid, since it builds directly upon EDFT, one of the most successful theories for the equilibrium properties of inhomogeneous fluids. As the presentation above shows, the DDFT is clearly not an exact theory. However, the fact that, in principle, the equilibrium profiles obtained from the DDFT are almost exact leads one to expect that the theory should be reliable – at least when the fluid is not too far from equilibrium.

### 3. Application of the DDFT to the GCM

We argued in the previous section that the DDFT (20) should be a good theory for the dynamics of a colloidal fluid when the fluid is near to equilibrium, provided we have an accurate approximation for the excess Helmholtz free energy functional  $F_{ex}[\{\rho_i(\mathbf{r}, t)\}]$  for the fluid (we now use  $i, j$ , rather than  $q, q'$  to label the different species of colloids). In this section we shall demonstrate that in the case of a particular model fluid for which we *do* have an accurate Helmholtz free energy functional, the DDFT seems to be

reliable even for situations when the fluid is quite far from equilibrium and phenomena such as phase separation and interfacial adsorption (wetting) are present. Throughout we assume that the Brownian level of description (9) provides an accurate account of the underlying particle dynamics.

Dzubiella and Likos [11] applied the DDFT to a one-component model fluid in which the particles interact via a purely repulsive Gaussian potential, the Gaussian core model (GCM). Their choice of model fluid was motivated by the fact that a simple mean-field approximation for  $F_{ex}[\{\rho_i(\mathbf{r})\}]$  proves to be quite accurate for the equilibrium properties, and thus they were able to test whether the DDFT formulation (16) of dynamics is accurate. We shall say more about this model fluid below. Their strategy was to consider the inhomogeneous fluid confined in either a spherical cavity or a slit. They used EDFT to calculate the equilibrium density profile corresponding to a particular external potential and considered cases when the external potential suddenly changed (i.e., a parameter in the external potential was either increased or decreased). Using the density profile from the EDFT as the starting density profile, they used the DDFT to determine how the density profile of the fluid evolved towards equilibrium. The reliability of their results was assessed by making comparison with BD simulation results – i.e. they numerically integrated Eq. (9) a number of different times, for different realisations of the stochastic noise, and then averaged over all the different runs in order to obtain the ensemble average time evolution of the fluid density profile. Dzubiella and Likos found that the DDFT and the BD simulation results were in very good agreement [11]. We follow the same strategy here but for a binary mixture of GCM particles.

The one component GCM does not exhibit fluid-fluid phase separation [3, 19]. It is therefore of interest to find out whether the DDFT proves to be reliable for the dynamics of inhomogeneous fluids when there is phase separation in the fluid and when related interfacial phenomena such as wetting of the cavity wall are present. The model fluid we consider is the binary GCM. This fluid does exhibit liquid-liquid phase separation [20, 21]. The GCM particles interact via the following purely repulsive pair potential:

$$u_{i,j}(r) = \epsilon_{i,j} \exp(-r^2/R_{i,j}^2) \quad (25)$$

and no other higher body potentials. In Eq. (25)  $i, j = 1, 2$  label the two different species of particles,  $\epsilon_{i,j} > 0$  is a parameter that determines the strength of the interaction and  $R_{i,j}$  denotes the range of the interaction potential. Note that this potential has no hard core; the centres of the particles can overlap completely. When one considers the effective potential between the centres of mass of polymers in a good solvent, one finds that the Gaussian potential (25), with  $\epsilon_{i,j} \sim 2k_B T$  and  $R_{i,j} \sim R_g$ , the polymer radius of gyration, provides a good approximation [3, 12, 13, 14, 15, 16]. When the fluid density becomes sufficiently high, each GCM particle interacts with a large number of neighbours, and it is established that the following mean-field excess Helmholtz free energy functional [3, 19, 20, 21]:

$$F_{ex}[\{\rho_i(\mathbf{r})\}] = \frac{1}{2} \sum_{i,j=1}^2 \int d\mathbf{r} \int d\mathbf{r}' \rho_i(\mathbf{r}) \rho_j(\mathbf{r}') u_{i,j}(|\mathbf{r} - \mathbf{r}'|), \quad (26)$$



becomes rather accurate. This functional generates the RPA closure for the direct pair correlation functions (c.f. Eq. (7)):

$$c_{i,j}^{(2)}(\mathbf{r}, \mathbf{r}') \equiv -\beta \frac{\delta^2 F_{ex}[\{\rho_i(\mathbf{r})\}]}{\delta \rho_i(\mathbf{r}) \delta \rho_j(\mathbf{r}')} = -\beta u_{i,j}(|\mathbf{r} - \mathbf{r}'|). \quad (27)$$

We solve the DDFT (20) for the binary GCM confined in spherically symmetric external potentials of the form:

$$u_{ext}^i(r) = E (r/\mathcal{R})^{10}, \quad (28)$$

where  $r$  is the distance from the origin,  $E = 10k_B T$  and the length-scale  $\mathcal{R}$  is the same for both species of particles. This potential is of the same form as one of the external potentials considered in Ref. [11] for a one component fluid of GCM particles. As the length parameter  $\mathcal{R}$  is increased, the size of the cavity is increased. We consider cases where for times  $t < 0$  the fluid is at equilibrium confined in a cavity with potentials (28), with  $\mathcal{R} = \mathcal{R}_1$ . Then at  $t = 0$  the cavity potentials change to ones with  $\mathcal{R} = \mathcal{R}_2 \neq \mathcal{R}_1$ . Due to the spherical symmetry of the external potentials, the (ensemble average) fluid one body density profiles will also display spherical symmetry. In the binary GCM fluid we shall consider mixtures with two different sets of pair potential parameters. The first corresponds to a set giving bulk liquid-liquid phase separation and the second to a set giving microphase-separation [23]. We shall also assume throughout that the friction constants for the two different species of particles are equal, i.e.,  $\Gamma_1^{-1} = \Gamma_2^{-1} = \Gamma^{-1}$ , to keep the problem as simple as possible. ¶

### 3.1. DDFT for a GCM fluid which exhibits bulk phase separation

We consider a binary GCM fluid with pair potential parameters  $\epsilon_{11} = \epsilon_{22} = 2k_B T$ ,  $\epsilon_{12} = 1.8877k_B T$ ,  $R_{22} = 0.665R_{11}$  and  $R_{12} = 0.849R_{11}$ , which exhibits bulk fluid-fluid phase separation. The fact that  $R_{12} = (1 + \Delta)(R_{11} + R_{22})/2$ , with  $\Delta > 0$ , ensures that the fluid exhibits positive non-additivity and it is this feature which induces phase separation. This choice of pair potential parameters was used in a number of previous studies by the author [21, 22, 33, 34, 35]. The fluid phase-separates at high total densities  $\rho = \rho_1 + \rho_2$ , where  $\rho_1$  and  $\rho_2$  are the bulk densities of the two species. Within the mean-field DFT defined by Eq. (26) the (lower) critical point is at  $\rho R_{11}^3 = 5.6$  and concentration  $x \equiv \rho_2/\rho = 0.70$  [21].

The first case we consider is that with  $N_1 = 200$  big particles of species 1 and  $N_2 = 100$  particles of species 2, confined in a cavity with  $\mathcal{R} = 4R_{11}$  for  $t < 0$ . At  $t = 0$  the cavity size is suddenly reduced to  $\mathcal{R} = 3R_{11}$ . In Fig. 1 we display the evolution of the fluid density profiles after this sudden compression of the cavity. We display the results from solving the DDFT (20) combined with the RPA functional (26), as well as results from BD simulations [36]. In the BD simulations we numerically integrate Eq. (9) generalised to two different species of GCM particles. We typically perform

¶ Another more realistic choice, following Stokes, would be to set  $\Gamma_i^{-1} \propto R_{ii}$ . However, we do not believe making this alternative choice would affect any of our overall conclusions.

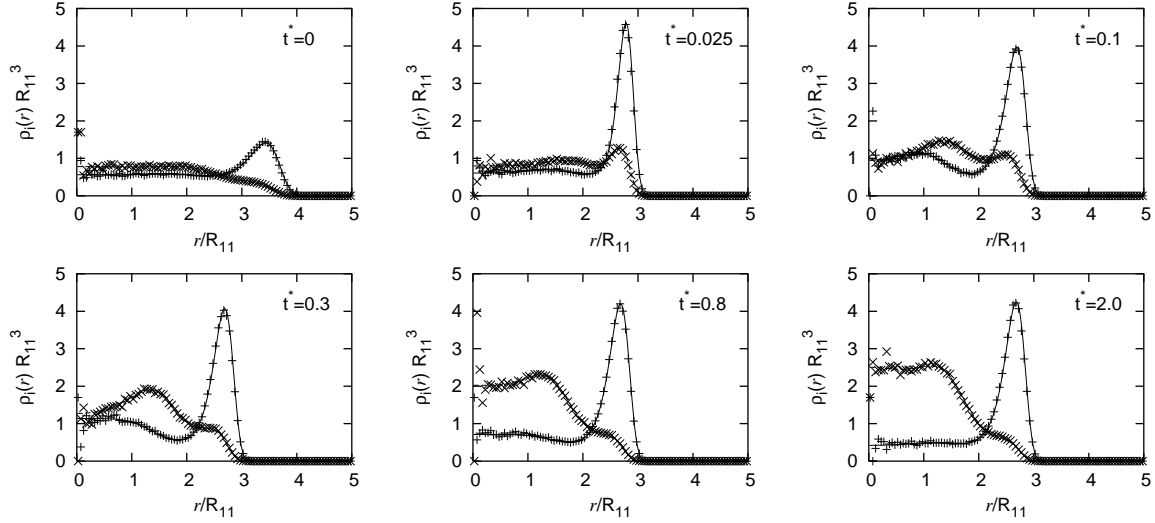


**Figure 1.** Density profiles  $\rho_i(r, t)$  (DDFT results: solid line for species 1, dashed line for species 2; symbols are BD results, (+) for species 1, (x) for species 2) for a fluid composed of  $N_1 = 200$  particles of species 1 and  $N_2 = 100$  particles of species 2, which is initially ( $t < 0$ ) at equilibrium in an external potential of the form in Eq. (28) with  $\mathcal{R} = 4R_{11}$ . At  $t = 0$  the external potentials suddenly change to those with  $\mathcal{R} = 3R_{11}$ . The profiles are plotted for various  $t^* = k_B T \Gamma R_{11}^2 t$ . The two species of particles are uniformly mixed in the cavity at  $t = 0$ , but due to the increase in density, the equilibrium profiles for the fluid in the cavity with  $\mathcal{R} = 3R_{11}$  exhibits a degree of demixing. Note also that  $\rho_1(r = 0, t)$  is a non-monotonic function of time.

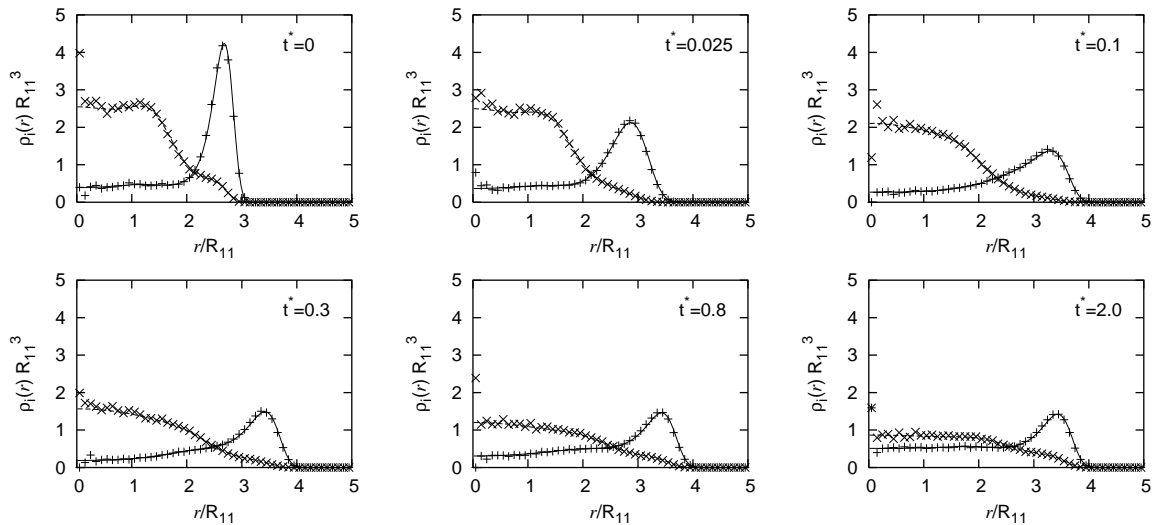


**Figure 2.** This is the reverse case of that displayed in Fig. 1. Initially ( $t < 0$ ) the fluid is at equilibrium confined in external potentials of the form Eq. (28) with  $\mathcal{R} = 3R_{11}$ . Then at  $t = 0$  the cavity potentials suddenly change to those with  $\mathcal{R} = 4R_{11}$ . The profiles are plotted for various  $t^* = k_B T \Gamma R_{11}^2 t$ .

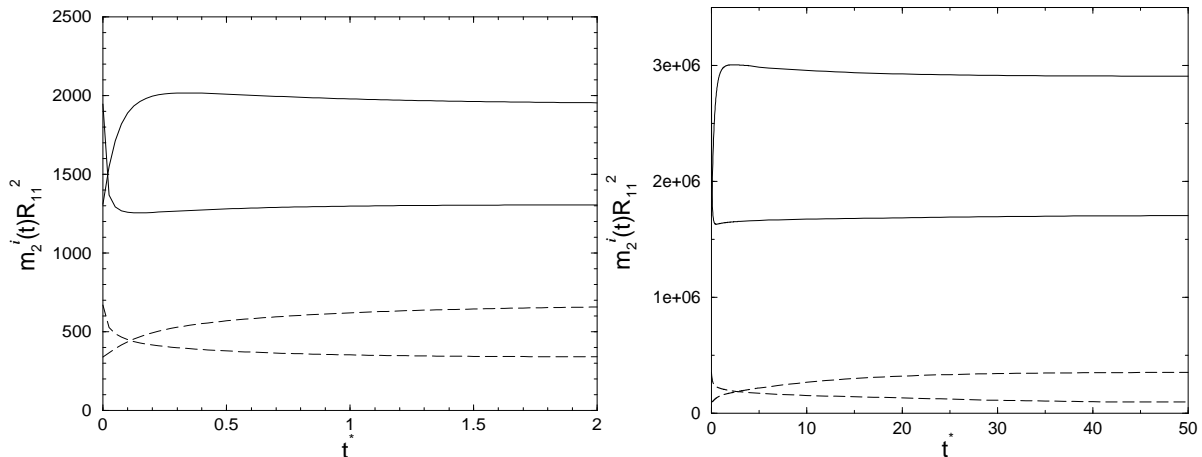


**Figure 3.** The second moment of the density profiles,  $m_2^i(t)$ , defined by Eq. (29). The left hand figure is for the cases corresponding to the density profiles displayed in Figs. 1 and 2. The right hand figure corresponds to the cases in Figs. 4 and 5. The solid lines are the second moment for species 1,  $m_2^1(t)$ , and the dashed lines  $m_2^2(t)$ , for species 2. In each case, the curves with a higher value of  $m_2^i(t \rightarrow \infty)$  correspond to a final external potential with a larger value of  $\mathcal{R}$ . Note that in both cases  $m_2^1(t)$  is non-monotonic, whereas  $m_2^2(t)$  is a monotonic function of time.

1500 different runs, each with different realisations of the stochastic noise term, and then average over all the different runs in order to obtain the ensemble average time evolution of the fluid density profiles. In order to generate each starting configuration, we allow the fluid to equilibrate for a reduced time  $t^* \equiv k_B T \Gamma R_{11}^2 t = 10$  with a fixed parameter  $\mathcal{R} = \mathcal{R}_1 (= 4R_{11})$  in the external potential, before changing this parameter to  $\mathcal{R} = \mathcal{R}_2 (= 3R_{11})$  and determining the relaxation of the fluid. In Fig. 1 the density profiles at  $t = 0$  correspond to those of the equilibrium fluid in a cavity with  $\mathcal{R} = 4R_{11}^+$ . When the external potential parameter  $\mathcal{R} = 4R_{11}$ , the two species of GCM particles are mixed within the cavity, although because the walls of the cavity favour species 1, there is a higher density of species 1 around the outside of the cavity. This preference of the cavity wall for species 1 is due to the fact that the cavity wall potentials for both species of particles decay into the fluid with the same decay length. This results in an effective attraction between the wall and species 1 [22]. For small  $t > 0$ , the initial ‘compression’ of the fluid results in the growth of a sharp peak in the densities of both species around  $r \simeq \mathcal{R}_2 = 3R_{11}$ . This causes a density ‘wave’ to travel through the fluid into the centre of the cavity. The fluid reaches equilibrium at  $t^* \equiv t/\tau_B \simeq 1.3$ , where  $\tau_B = \beta/\Gamma R_{11}^2$  is the Brownian time scale. In Fig. 1 we display the fluid density profiles for the times  $t^* = 0, 0.025, 0.1, 0.3, 0.8$ , and 2. The profile for  $t^* = 2$  effectively corresponds to the equilibrium profile for the external potential (28) with  $\mathcal{R} = 3R_{11}$ . With this value of  $\mathcal{R}$  the fluid exhibits a degree of phase separation in the cavity due to the fact that the total

<sup>+</sup> Note that within the grand canonical EDFT the *mean* number of particles  $\langle N_i \rangle$  of species  $i$  in the cavity is constrained. In practice we set the chemical potentials  $\mu_i$  such that the the mean number of particles in the cavity,  $\langle N_i \rangle = \int d\mathbf{r} \rho_i(\mathbf{r}) = N_i$ , the number of particles in the BD simulation.

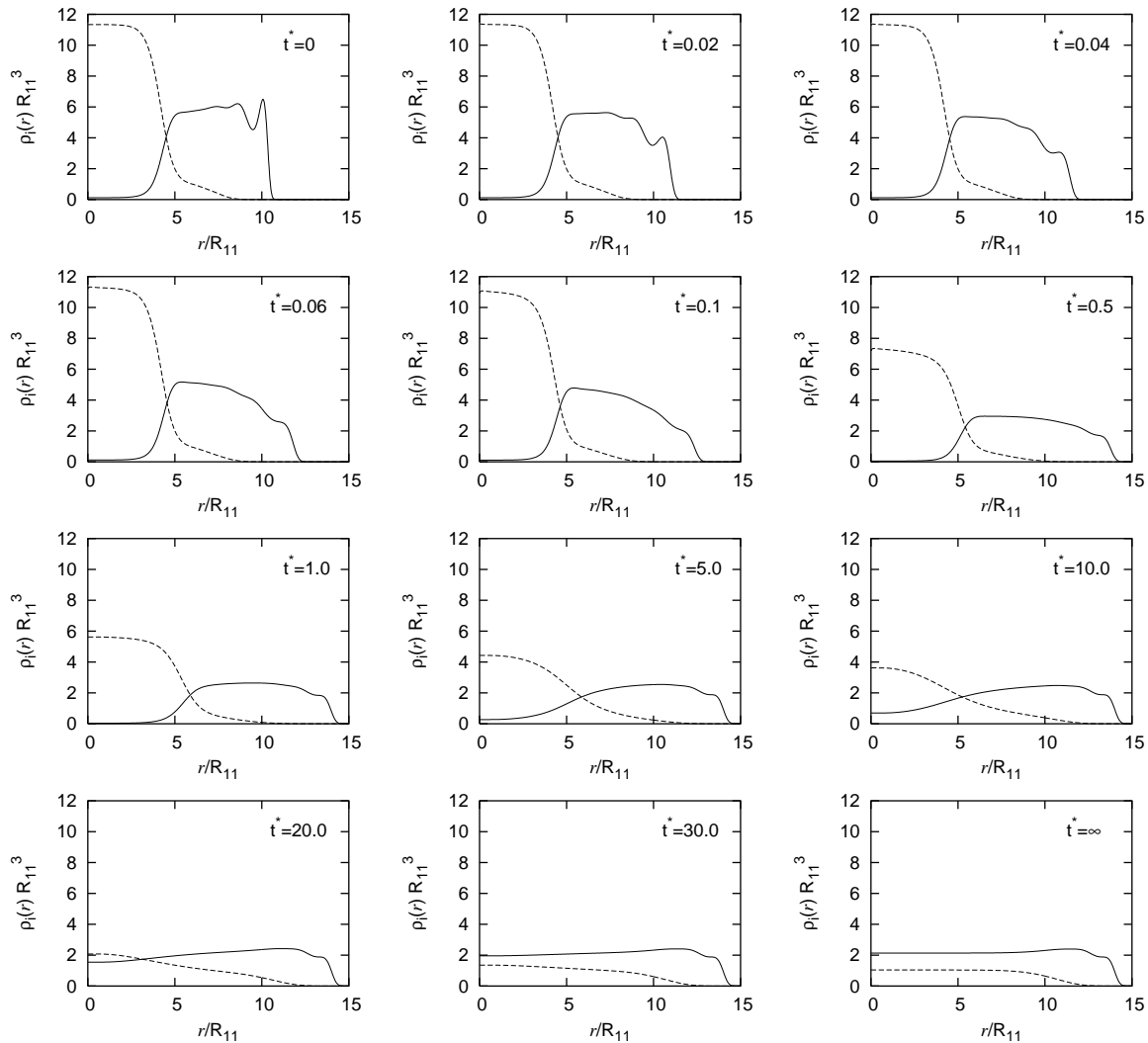


**Figure 4.** Density profiles  $\rho_i(r, t)$  (solid line for species 1, dashed line for species 2) for a fluid composed of  $N_1 = 25000$  particles of species 1 and  $N_2 = 5000$  particles of species 2, which is initially ( $t < 0$ ) at equilibrium confined in external potentials of the form in Eq. (28) with  $\mathcal{R} = 9R_{11}$ . Then at  $t = 0$  the external potentials suddenly change to those with  $\mathcal{R} = 13R_{11}$ . The profiles are plotted for various  $t^* = k_B T \Gamma R_{11}^2 t$ . Initially, the fluid is separated into two phases, one rich in species 1 around the outside, ‘wetting’ the wall of the cavity, and the other phase in the centre of the cavity, rich in species 2. Notice the slow diffusion of particles through the fluid-fluid interface in the later stages of the equilibration.

density of the fluid in the cavity has increased. The particles of species 1 are mostly to be found adsorbed around the wall of the cavity and species 2 towards the centre of the cavity. In Fig. 2 we display the density profiles for the reverse situation to the case in Fig. 1: The external potentials (28) are initially ( $t < 0$ ) those with  $\mathcal{R} = 3R_{11}$ . Then, at  $t = 0$ , the potentials are changed to those with  $\mathcal{R} = 4R_{11}$ . In this case the fluid reaches equilibrium when  $t^* \simeq 1.7$ . The reason that the ‘compression’ case (Fig. 1) is able to reach equilibrium faster than the relaxation case (Fig. 2) is that in the compression

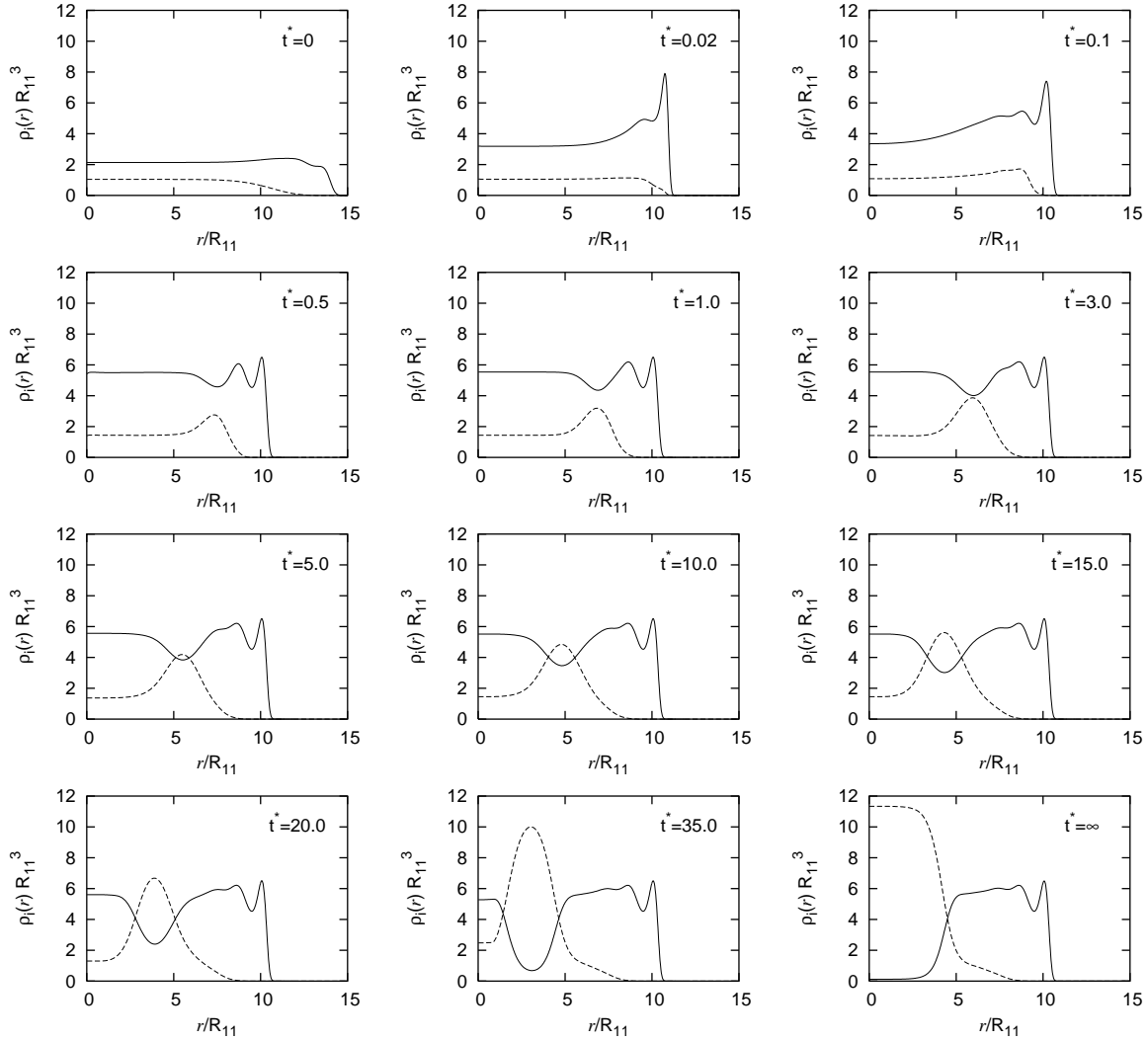


**Figure 5.** This is the reverse case of that displayed in Fig. 4. Initially ( $t < 0$ ) the fluid is at equilibrium confined in external potentials of the form in Eq. (28) with  $\mathcal{R} = 13R_{11}$ . Then at  $t = 0$  the external potentials suddenly change to those with  $\mathcal{R} = 9R_{11}$ . The profiles are plotted for various  $t^* = k_B T \Gamma R_{11}^2 t$ . Notice the concentration ‘wave’ (dip in the profile of species 1 and a peak in profile for species 2) that travels towards the centre of the cavity which allows the fluid to reach equilibrium slightly faster than in the opposite (relaxation) process – see Fig. 4.

case the ‘shock wave’ that travels inward, mixes up the fluid, which allows it to reach equilibrium faster than in the relaxation case. In Fig. 3 we display the second moment of the density profile,

$$m_2^i(t) = \int d\mathbf{r} r^2 \rho_i(\mathbf{r}, t). \quad (29)$$

Dzubiella and Likos [11] found that for a one component GCM fluid this is a monotonic function of time. For the relaxation (cavity expansion) case they found that  $m_2(t)$  can be very accurately approximated by an exponentially decaying function. For the

compression case,  $m_2(t)$  is also monotonic, and can be accurately parameterised by a function composed of two exponentials. They also found that the one component GCM fluid reaches equilibrium faster in the compression case, where  $\mathcal{R}$  is decreased at time  $t = 0$ , rather than the relaxation case. For the binary GCM fluid,  $m_2^2(t)$  is also a monotonic function of time (dashed lines), but interestingly,  $m_2^1(t)$  is not (solid lines) – see Fig. 3. This is because particles of species 1 are adsorbed on the wall of the cavity and when the parameter  $\mathcal{R}$  in the external potentials is suddenly decreased, particles of species 1 are forced more strongly towards the centre of the cavity than the species 2 particles. This causes an increase in the density of species 1 at the centre of the cavity. However, in the final stages of the fluid equilibration, the density of species 1 at the centre of the cavity decreases again. In other words,  $\rho_1(r = 0, t)$  is a non-monotonic function of time. Similarly, when the cavity is suddenly increased in size, it is the particles of species 1 that ‘feel’ the space around the outside of the fluid that has suddenly appeared, rather than the species 2 particles, and so it is species 1 particles that move outwards to fill this space. However, in the final stages of the fluid equilibration process, there is a net flow of species 1 particles back towards the centre of the cavity. For these reasons, only  $m_2^1(t)$  is a non-monotonic function of time. Dynamic processes such as these only occur when the fluid confined in the cavity is a binary fluid, where the wall of the cavity has a preference for one of the species. As can be seen from Figs. 1 and 2 there is remarkably good agreement between the density profiles obtained from the DDFT and from the BD simulations. This agreement gives us confidence concerning the reliability of the DDFT for cases where the numbers of particles are such that BD simulations become computationally too expensive. Note also that the RPA functional (26) becomes increasingly accurate as the GCM fluid density is increased [3, 19]; this should further improve the accuracy of the DDFT results.

In Figs. 4 and 5 we display the DDFT results for a similar situation as in Figs. 1 and 2, except in this case the cavity is larger and the number of confined particles is higher:  $N_1 = 25000$  particles of species 1 and  $N_2 = 5000$  particles of species 2 (the average densities are also higher). In Fig. 4 we display the results for the case when the fluid, for  $t < 0$ , is at equilibrium in a cavity with potentials given by Eq. (28) with  $\mathcal{R} = 9R_{11}$ . Then at  $t = 0$  the potentials change suddenly to those with  $\mathcal{R} = 13R_{11}$ . We plot the density profiles for  $t^* = 0, 0.02, 0.04, 0.06, 0.1, 0.5, 1, 5, 10, 20, 30$  and  $\infty$ . (Here and elsewhere, the  $t = \infty$  density profiles are those obtained using EDFT for cavity potentials with  $\mathcal{R} = \mathcal{R}_2$ . In the present case  $\mathcal{R}_2 = 13R_{11}$ .) We see that at  $t = 0$  the fluid is strongly phase separated in the cavity, with the phase rich in species 1 ‘wetting’ the wall of the cavity, and the phase rich in species 2 at the centre of the cavity. The final equilibrium configuration,  $t \rightarrow \infty$ , when the cavity radius  $\mathcal{R} = 13R_{11}$ , is that where the two species of particles are mixed together in the cavity, although the preference of the cavity wall for species 1 ensures that the density of species 1 is still higher around the outside of the cavity. In order to reach this equilibrium configuration the fluid first exhibits a ‘quick’ flow of the phase rich in species 1 to fill the space created around the outside of the fluid by the cavity expansion. There is then a second ‘slow’

process whereby the two demixed phases mix, i.e. the diffusion of particles across the fluid-fluid interface is a slow process.

For the reverse (cavity compression) situation, the results are displayed in Fig. 5. For  $t < 0$  the fluid is at equilibrium in a cavity with potentials given by Eq. (28) with  $\mathcal{R} = 13R_{11}$ . Then at  $t = 0$  the potentials change suddenly to those with  $\mathcal{R} = 9R_{11}$ . We plot the density profiles for  $t^* = 0, 0.02, 0.1, 0.5, 1, 3, 5, 10, 15, 20, 35$  and  $\infty$ . In this case the fluid reaches equilibrium slightly faster than in the case where the cavity size is increased. This is because in the cavity compression case, the sudden decrease of  $\mathcal{R}$  at  $t = 0$  sends a particle concentration ‘wave’ into the centre of the cavity (see Fig. 5) which allows the fluid to reach equilibrium faster. This ‘wave’ forms as a dip in the density profile of species 1 and a peak in profile for species 2 couple together and move towards the centre of the cavity. The amplitude of the wave increases with proximity to the centre of the cavity. As can be seen in the right hand figure of Fig. 3 for both these cases the second moments of the density profiles, given by Eq. (29), show similar behaviour to the cases with fewer particles in Figs. 1 and 2 – see Fig. 3.  $m_2^1(t)$  is a non-monotonic function of time, whereas  $m_2^2(t)$  is a monotonic function of time. As for the cases in Figs. 1 and 2, this is due to the fact that the species 1 particles are adsorbed on the cavity wall, rather than the species 2 particles.

### 3.2. DDFT for a GCM fluid which exhibits microphase separation

We now consider a binary GCM fluid with pair potential parameters the same as in the previous subsection except that  $R_{12} = 0.6R_{11}$ , i.e.  $R_{12} = (1 + \Delta)(R_{11} + R_{22})/2$ , with  $\Delta < 0$ ; the fluid exhibits negative non-additivity. This fluid does not exhibit bulk fluid-fluid phase separation. Due to the negative non-additivity there is a propensity to ordering in the fluid in which particles of species 1 have as nearest neighbours particles of species 2, and vice versa [23]. We refer to this phenomenon as ‘1-2 ordering’. At high total densities EDFT predicts that this GCM fluid freezes into a crystal in which the particles are highly delocalized, with Lindemann parameters as high as 90% near melting [23]. When the fluid is confined in a spherical cavity and the fluid density is high enough, the fluid forms an ‘onion’ structure of alternating layers, one particle thick, of the two different species [23] (see also Figs. 6, 7, 9 and 10). Similarly, when the high density mixture is confined in a planar slit the density profiles show that fluid forms alternating layers of the two different species parallel to the walls of the slit [23]. At lower densities the two different species of particles are mixed. This microphase separation is associated with the fact that the bulk fluid exhibits an instability with respect to periodic density modulations – a ‘ $\lambda$ -instability’. For more details regarding the origin of this instability see Ref. [23] and references therein. Here our interest is limited to the question: Can the DDFT describe the formation of ‘onion’ structures in a spherical cavity with potentials given by Eq. (28) when  $\mathcal{R}$  is reduced, and can the DDFT describe the onion ‘melting’ when  $\mathcal{R}$  is increased?

We follow a strategy similar to that taken in the previous subsection and make

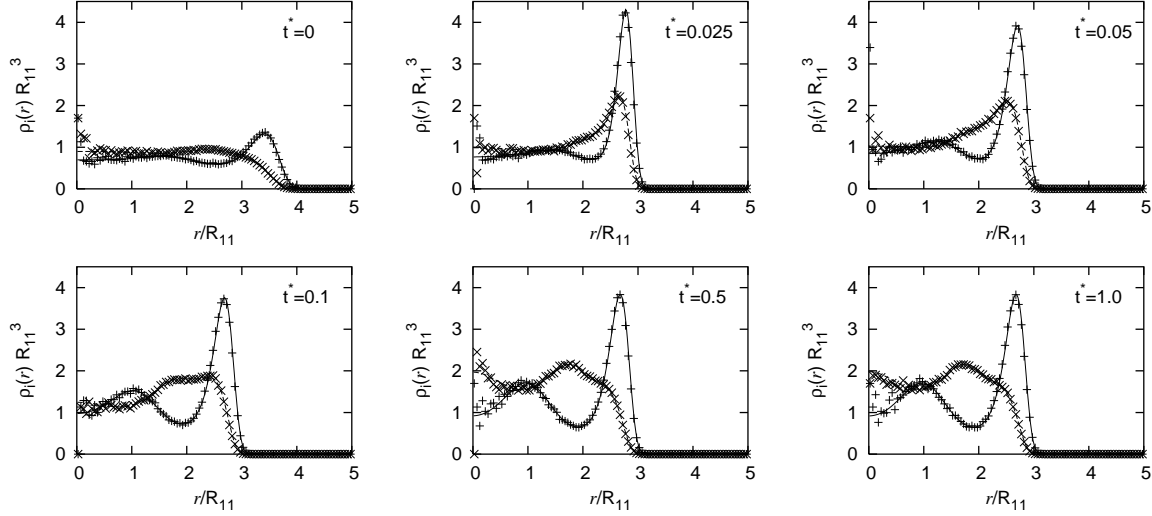


**Figure 6.** Density profiles  $\rho_i(r, t)$  (solid line is DDFT results for species 1, dashed line for species 2; symbols are BD results, (+) for species 1, (x) for species 2.) for a fluid composed of  $N_1 = 200$  particles of species 1 and  $N_2 = 150$  particles of species 2, which is initially ( $t < 0$ ) at equilibrium confined in external potentials of the form in Eq. (28) with  $\mathcal{R} = 4R_{11}$ . Then at  $t = 0$ , the external potentials suddenly change to those with  $\mathcal{R} = 3R_{11}$ . The profiles are plotted for various  $t^* = k_B T \Gamma R_{11}^2 t$ . This model fluid exhibits microphase-separation. The final  $t^* = 1$  configuration is an ‘onion’ structure.

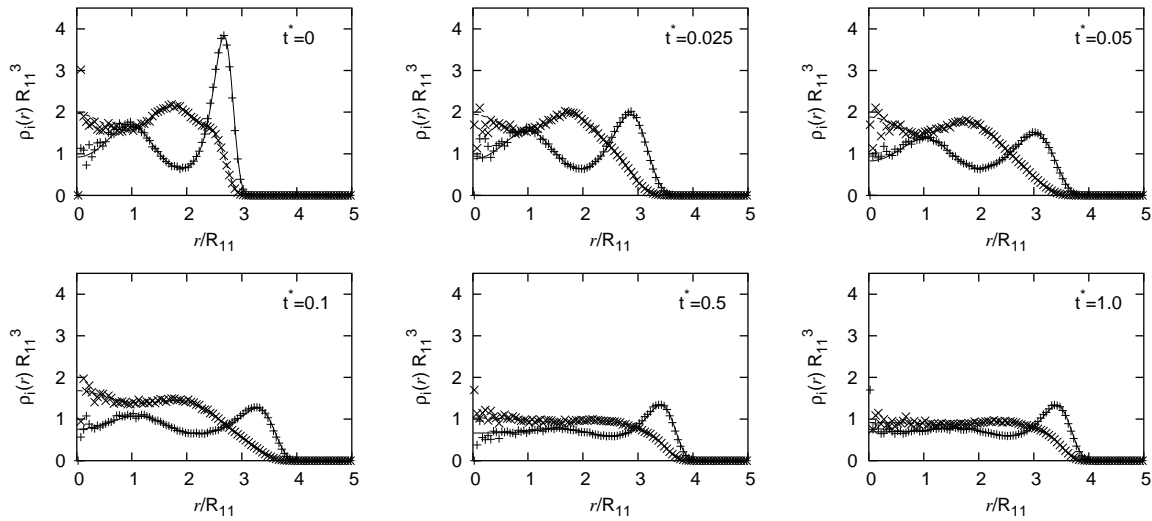


**Figure 7.** This is the reverse case of that displayed in Fig. 6. Initially ( $t < 0$ ) the fluid is at equilibrium confined in external potentials of the form in Eq. (28) with  $\mathcal{R} = 3R_{11}$ . Then at  $t = 0$ , the external potentials suddenly change to those with  $\mathcal{R} = 4R_{11}$ . The profiles are plotted for various  $t^* = k_B T \Gamma R_{11}^2 t$ . The initial  $t = 0$  configuration is an ‘onion’ structure.



a comparison between the results from DDFT and BD simulations for cases with a limited number of particles, in order to demonstrate the reliability of the DDFT for this particular GCM fluid and then we apply the DDFT to cases where the number of particles is too high for simulations to be a realistic tool for studying the dynamics. In Fig. 6 we display the density profiles for a fluid composed of  $N_1 = 200$  particles of species 1 and  $N_2 = 150$  particles of species 2, which is initially ( $t < 0$ ) at equilibrium confined in external potentials of the form in Eq. (28) with  $\mathcal{R} = 4R_{11}$ . Then at  $t = 0$  the external potentials are suddenly changed to those with  $\mathcal{R} = 3R_{11}$ . We display the density profiles for  $t^* = 0, 0.025, 0.05, 0.1, 0.5$  and  $1$ . In the initial  $t = 0$  density profiles we see that there is little sign of the fluid exhibiting 1-2 ordering. As was the case for the fluid described in the previous subsection, the wall potentials result in an effective attraction between the wall of the cavity and particles of species 1. Therefore there is an increased density of species 1 around the wall of the cavity. Following the compression in the cavity at  $t = 0$ , there is an initial in-flow of fluid towards the centre of the cavity and an increase in the density of the fluid near to the cavity wall. Following this initial stage, the fluid relaxes into a configuration which exhibits a pronounced degree of 1-2 ordering – see the  $t^* = 1$  figure in Fig. 6. In Fig. 7 we display the results for the reverse situation, i.e. when the fluid is initially ( $t < 0$ ) at equilibrium confined in external potentials of the form in Eq. (28) with  $\mathcal{R} = 3R_{11}$ , then at  $t = 0$ , the external potentials suddenly change to those with  $\mathcal{R} = 4R_{11}$ . We display the profiles for  $t^* = 0, 0.025, 0.05, 0.1, 0.5$  and  $1$ . In both cases the agreement between the DDFT and the BD simulations is remarkably good. Fig. 8 displays the results for the second moment of the density profile, defined by Eq. (29). As in the previous subsection, in the present case the moments  $m_2^1(t)$  for species 1 are non-monotonic functions of time, whereas the moments  $m_2^2(t)$  are monotonic functions of time. The fluid which exhibits 1-2 ordering is able to reach equilibrium faster than the fluid considered in the previous subsection which exhibits bulk phase separation. This is because the average distance the particles must diffuse to be arranged in a microphase-separated distribution is shorter than in the case where the final equilibrium configuration is that exhibiting ‘bulk’ phase-separation. In the latter case the particles of species 1 must diffuse to the outside of the cavity, whilst particles of species 2 must diffuse to the centre of the cavity in order to reach equilibrium.

In Figs. 9 and 10 we display the DDFT results for a similar situation, except now the cavity is larger and the number of confined particles is also much bigger:  $N_1 = 16000$  particles of species 1 and  $N_2 = 15000$  particles of species 2 (the average densities are also higher). In Fig. 9 we display the results for the case when the fluid, for  $t < 0$ , is at equilibrium in a cavity with potentials given by Eq. (28) with  $\mathcal{R} = 8R_{11}$ . Then at  $t = 0$  the potentials change suddenly to those with  $\mathcal{R} = 10R_{11}$ . We plot the density profiles for  $t^* = 0, 0.02, 0.06, 0.1, 0.2, 0.5, 0.7, 1$  and  $\infty$ . At  $t = 0$  the two different species of particles are strongly ordered into alternating layers of the two different species – an ‘onion’ structure. The final equilibrium configuration,  $t \rightarrow \infty$ , is that where the two species of particles are uniformly mixed in the cavity, although, due to the preference of the cavity wall for species 1, the density of species 1 is higher in the outer region of

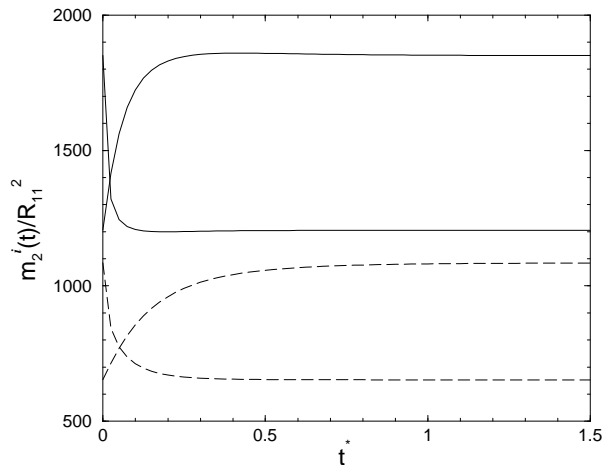


**Figure 8.** The second moment of the density profiles,  $m_2^i(t)$ , defined by Eq. (29), for a GCM fluid exhibiting microphase-separation, with density profiles displayed in Figs. 6 and 7. The solid lines are the second moment for species 1,  $m_2^1(t)$ , and the dashed lines  $m_2^2(t)$ , for species 2. In each case, the curves with a higher value of  $m_2^i(t \rightarrow \infty)$  correspond to a final external potential with a larger value of  $\mathcal{R}$ . Note that in both cases  $m_2^1(t)$  is non-monotonic, whereas  $m_2^2(t)$  is a monotonic function of time, as was the case in Fig. 3 for a GCM fluid that exhibits bulk phase separation.

the cavity. The equilibration process is almost an order of magnitude shorter in time than in either of the cases in Figs. 4 or 5 for the GCM fluid exhibiting bulk liquid-liquid phase separation, even though the number of particles involved in these cases is similar. This is because the particles must diffuse a distance  $\sim R_{11}$ , the particle size, in order to go from a state with 1-2 ordering to a mixed state, whereas for the fluid exhibiting ‘bulk’ phase separation the particles must diffuse a much larger distance  $\sim \mathcal{R}$ , the radius of the cavity. For the reverse (cavity compression) situation, the results are displayed in Fig. 10. Initially, for  $t < 0$ , the fluid is at equilibrium in a cavity with potentials given by Eq. (28) with  $\mathcal{R} = 10R_{11}$ . Then at  $t = 0$  the potentials change suddenly to those with  $\mathcal{R} = 8R_{11}$ . We plot the density profiles for  $t^* = 0, 0.01, 0.02, 0.06, 0.1, 0.2, 0.5, 0.7$  and  $\infty$ . As with the cavity expansion case in Fig. 9 this process is almost an order of magnitude quicker in time than in either of the cases in Figs. 4 or 5. The compression causes the total fluid density to first increase around the wall of the cavity, before increasing near the centre of the cavity. This results in the ‘onion’ layers forming first in the outer region and then developing inwards towards the centre of the cavity as the fluid equilibrates.

#### 4. Liouville, Kramers and Smoluchowski equations

We now turn to the question of what approximations are involved in the present description of the fluid dynamics. Under what circumstances can the equations of motion for a solution of colloids suspended in a solvent of much smaller particles be

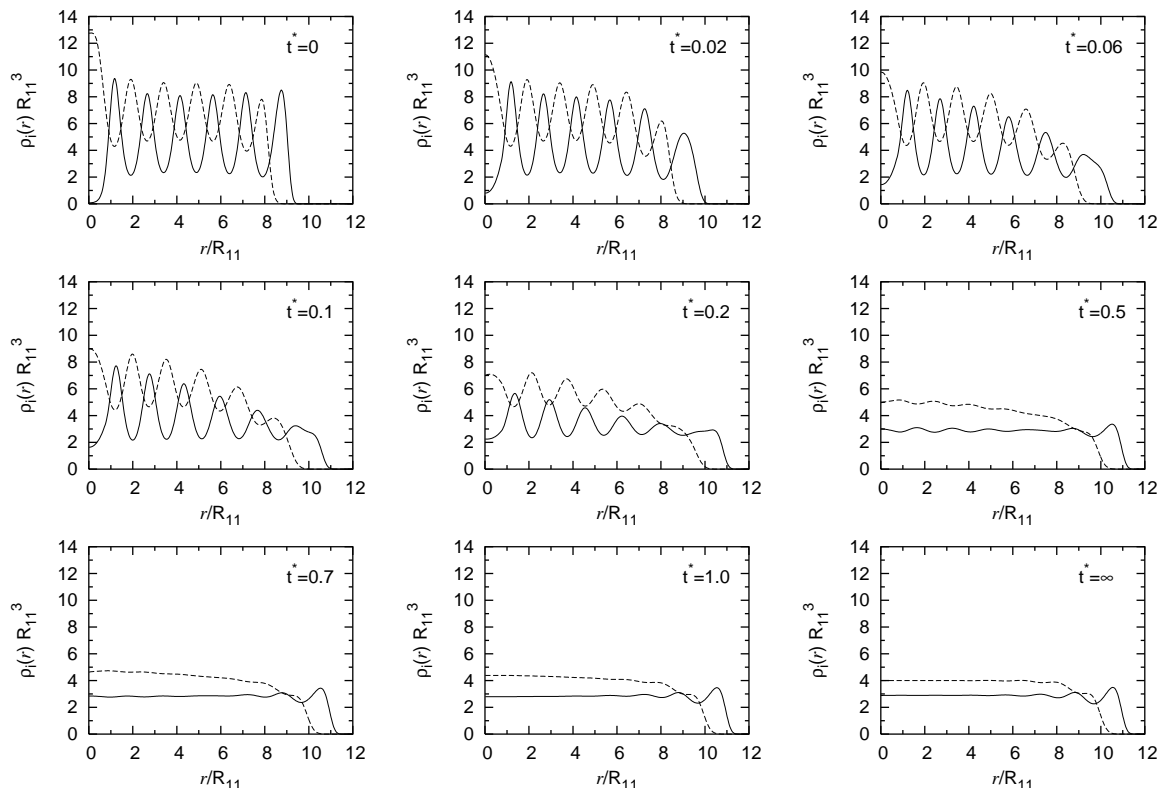


**Figure 9.** Density profiles  $\rho_i(r, t)$  (solid line for species 1, dashed line for species 2) for a fluid composed of  $N_1 = 16000$  particles of species 1 and  $N_2 = 15000$  particles of species 2, which is initially ( $t < 0$ ) is at equilibrium confined in external potentials of the form in Eq. (28) with  $\mathcal{R} = 8R_{11}$ . Then at  $t = 0$  the external potentials are suddenly changed to those with  $\mathcal{R} = 10R_{11}$ . The profiles are plotted for various  $t^* = k_B T \Gamma R_{11}^2 t$ . This model fluid exhibits microphase-separation. The initial  $t = 0$  configuration is an ‘onion’ structure.

approximated by the stochastic equations of motion (9)? Or, equivalently, in which situations can the time evolution of the probability density function for the full system of colloid and solvent particles be approximated by the Smoluchowski equation (11)? In Refs. [37, 38] these questions are addressed for the case of a fluid in which one of the particles is much larger than the rest and when the solvent friction coefficient  $\Gamma^{-1}$  is sufficiently large, that one can argue that the time evolution of the probability distribution function for the single big (colloid) particle is governed by the single particle Smoluchowski equation. Here we present an argument which is a simplified generalisation (for  $N$  big colloid particles) of this argument. The derivation does not contain new ideas. However, we do make connections between older, well known, results concerning the dynamics of colloidal fluids and more recent developments in the theory of solvent mediated effective potentials between colloids in solution [3]. The following therefore provides much insight to the physics incorporated in the Smoluchowski equation and therefore also in the DDFT, and applies generally to colloidal fluids.

We consider a fluid consisting of a single species of  $N$  colloid particles of mass  $m$ ,

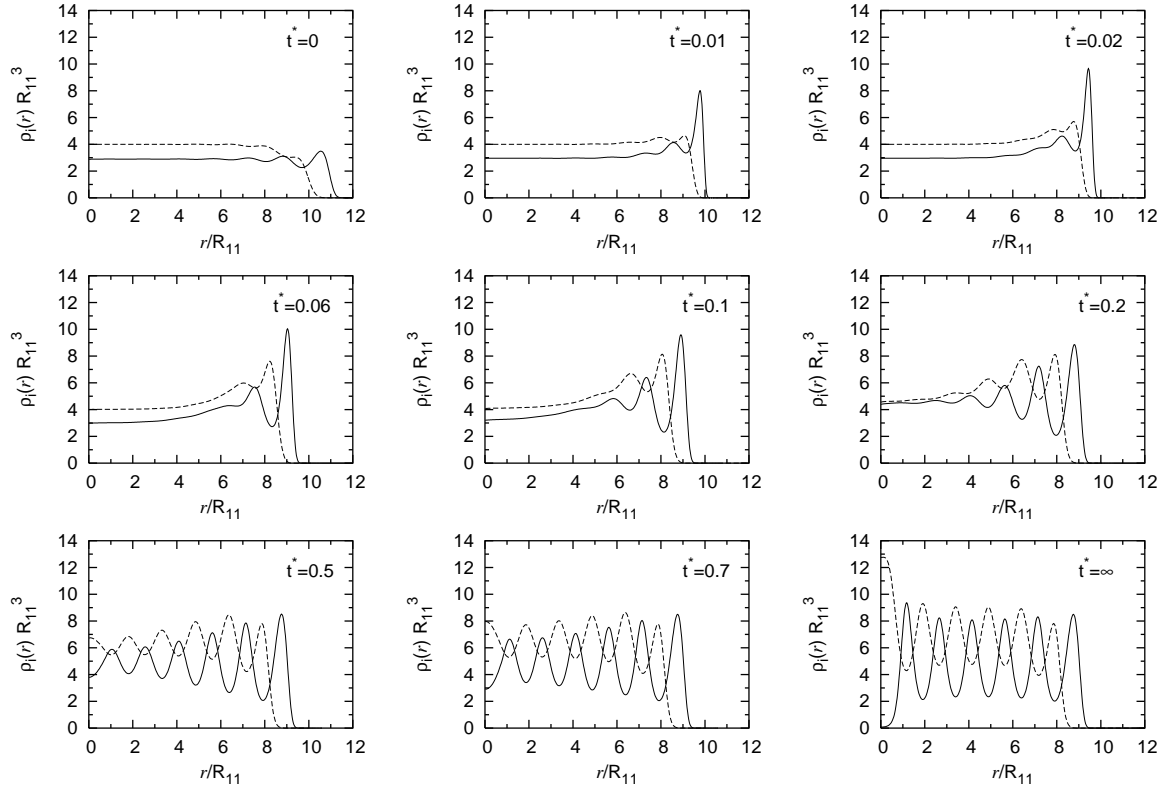


**Figure 10.** This is the reverse case of that displayed in Fig. 9. Initially ( $t < 0$ ) the fluid is at equilibrium confined in external potentials of the form in Eq. (28) with  $\mathcal{R} = 10R_{11}$ . Then at  $t = 0$ , the external potentials suddenly change to those with  $\mathcal{R} = 8R_{11}$ . The density profiles (solid line for species 1, dashed line for species 2) are plotted for various  $t^* = k_B T \Gamma R_{11}^2 t$ .

suspended in a single component solvent composed of  $S$  solvent particles, of mass  $M$ . We denote the coordinates of the  $i^{\text{th}}$  colloid by  $\mathbf{r}_i$  and momentum  $\mathbf{p}_i$ . The set of colloid position coordinates we denote by  $\mathbf{r}^N \equiv \{\mathbf{r}_1, \dots, \mathbf{r}_N\}$  and similarly  $\mathbf{p}^N \equiv \{\mathbf{p}_1, \dots, \mathbf{p}_N\}$ . For the solvent particles we denote the location in phase space of the  $\nu^{\text{th}}$  solvent particle by  $(\mathbf{R}_\nu, \mathbf{P}_\nu)$ . Just as for the colloids, we denote the sets  $\mathbf{R}^S \equiv \{\mathbf{R}_1, \dots, \mathbf{R}_S\}$  and  $\mathbf{P}^S \equiv \{\mathbf{P}_1, \dots, \mathbf{P}_S\}$ . The Hamiltonian for this system is:

$$\begin{aligned} \mathcal{H}(\mathbf{r}^N, \mathbf{p}^N, \mathbf{R}^S, \mathbf{P}^S, t) = & \frac{1}{2m} \sum_{i=1}^N |\mathbf{p}_i|^2 + \frac{1}{2M} \sum_{\nu=1}^S |\mathbf{P}_\nu|^2 \\ & + V_N(\mathbf{r}^N, t) + V_{N,S}(\mathbf{r}^N, \mathbf{R}^S) + V_S(\mathbf{R}^S, t), \end{aligned} \quad (30)$$

where the first two terms on the right hand side are the colloid and solvent kinetic energy contributions to the Hamiltonian.  $V_N(\mathbf{r}^N, t)$  is the colloid potential energy:

$$V_N(\mathbf{r}^N, t) = \sum_{i=1}^N v_{ext}(\mathbf{r}_i, t) + \frac{1}{2} \sum_{j \neq i} \sum_{i=1}^N v_2(\mathbf{r}_i, \mathbf{r}_j) + \frac{1}{6} \sum_{k \neq j \neq i} \sum_{j \neq i} \sum_{i=1}^N v_3(\mathbf{r}_i, \mathbf{r}_j, \mathbf{r}_k) + \dots \quad (31)$$

which is assumed to be made up of a one-body term (external potential  $v_{ext}(\mathbf{r}_i, t)$  on each colloid particle) a two-body term ( $v_2(\mathbf{r}_i, \mathbf{r}_j)$  is the pair potential), a three body

term  $v_3(\mathbf{r}_i, \mathbf{r}_j, \mathbf{r}_k)$ , etc. Note that  $V_N(\mathbf{r}^N, t)$  describes the *direct* or bare colloid-colloid interaction potential; it does not involve effective solvent mediated interactions and is therefore not the same as  $U_N(\mathbf{r}^N, t)$  in Eq. (8) – we will further clarify this issue later (see Eq. (43))\*. Similarly,  $V_S(\mathbf{R}^S, t)$  is the solvent potential energy and  $V_{N,S}(\mathbf{r}^N, \mathbf{R}^S)$  is the potential energy arising from interactions between the colloid and the solvent particles.

We can define a phase space probability density function  $f^{(N+S)}(\mathbf{r}^N, \mathbf{p}^N, \mathbf{R}^S, \mathbf{P}^S, t)$  for the fluid, and its time evolution is governed by the (exact) Liouville equation [29]:

$$\begin{aligned} \frac{\partial f^{(N+S)}}{\partial t} + \frac{1}{m} \sum_{i=1}^N \mathbf{p}_i \cdot \frac{\partial f^{(N+S)}}{\partial \mathbf{r}_i} + \sum_{i=1}^N \mathbf{X}_i \cdot \frac{\partial f^{(N+S)}}{\partial \mathbf{p}_i} + \frac{1}{M} \sum_{\nu=1}^S \mathbf{P}_\nu \cdot \frac{\partial f^{(N+S)}}{\partial \mathbf{R}_\nu} \\ + \sum_{\nu=1}^S \mathbf{Y}_\nu \cdot \frac{\partial f^{(N+S)}}{\partial \mathbf{P}_\nu} + \sum_{\nu=1}^S \bar{\mathbf{Z}}_\nu \cdot \frac{\partial f^{(N+S)}}{\partial \mathbf{P}_\nu} + \sum_{i=1}^N \mathbf{Z}_i \cdot \frac{\partial f^{(N+S)}}{\partial \mathbf{p}_i} = 0, \end{aligned} \quad (32)$$

where

$$\mathbf{X}_i = -\frac{\partial V_N}{\partial \mathbf{r}_i}, \quad \mathbf{Y}_\nu = -\frac{\partial V_S}{\partial \mathbf{R}_\nu}, \quad \mathbf{Z}_i = -\frac{\partial V_{N,S}}{\partial \mathbf{r}_i}, \quad \bar{\mathbf{Z}}_\nu = -\frac{\partial V_{N,S}}{\partial \mathbf{R}_\nu}, \quad (33)$$

are forces on the particles. The Liouville equation is a statement of the continuity of  $f^{(N+S)}$  in phase space over time.

Since the solvent particles are much smaller than the colloids, they will equilibrate on a time scale  $\tau_s$  much smaller than the time scale  $\tau_c$  on which the colloids equilibrate, i.e.  $\tau_c \gg \tau_s$ . We are interested in phenomena that occur on time scales  $\sim \tau_c$ , so we can assume that effectively the solvent particles equilibrate instantaneously, and when we integrate over the solvent degrees of freedom in Eq. (32) we obtain an equation similar to the Liouville equation for a one component fluid of  $N$  particles, but with an additional ‘solvent’ term due to interactions between the colloid and solvent particles:

$$\frac{\partial f^{(N)}}{\partial t} + \frac{1}{m} \sum_{i=1}^N \mathbf{p}_i \cdot \frac{\partial f^{(N)}}{\partial \mathbf{r}_i} + \sum_{i=1}^N \mathbf{X}_i \cdot \frac{\partial f^{(N)}}{\partial \mathbf{p}_i} = \left( \frac{\partial f^{(N)}}{\partial t} \right)_{\text{solvent}}, \quad (34)$$

where the colloid reduced probability density function is

$$f^{(N)}(\mathbf{r}^N, \mathbf{p}^N, t) \equiv \int d\mathbf{P}^S \int d\mathbf{R}^S f^{(N+S)}(\mathbf{r}^N, \mathbf{p}^N, \mathbf{R}^S, \mathbf{P}^S, t) \quad (35)$$

and formally the ‘solvent’ term is

$$\left( \frac{\partial f^{(N)}}{\partial t} \right)_{\text{solvent}} \equiv - \sum_{i=1}^N \frac{\partial}{\partial \mathbf{p}_i} \cdot \int d\mathbf{P}^S \int d\mathbf{R}^S \mathbf{Z}_i f^{(N+S)}. \quad (36)$$

The term  $\int d\mathbf{P}^S \int d\mathbf{R}^S \mathbf{Z}_i f^{(N+S)}$  in (36) is proportional to the average force exerted on colloid  $i$  by the solvent particles. On this ‘coarse-grained’ time scale  $\gg \tau_s$ , the leading order contributions to this force are a one body (Stokes) drag force on each colloid,

\* For generality we assume  $V_N(\mathbf{r}^N, t)$  contains higher body terms, although it is generally assumed that the bare interactions between particles are pairwise with no higher body terms. In principle, the higher-body terms arise from integrating over quantal degrees of freedom in obtaining  $V_N(\mathbf{r}^N, t)$ .

$-\gamma \mathbf{p}_i$ , where  $\gamma$  is a friction coefficient, and a force term,  $\mathbf{x}_i$ , due to solvent mediated interactions between the colloids. This force is

$$\mathbf{x}_i = -\frac{\partial \Phi_N}{\partial \mathbf{r}_i}, \quad (37)$$

where  $\Phi_N(\mathbf{r}^N)$  is the effective solvent mediated potential between the colloid particles. For an equilibrium fluid  $\Phi_N(\mathbf{r}^N) = -k_B T \ln Q_S(\mathbf{r}^N)$ , where  $Q_S(\mathbf{r}^N)$  is a partial partition function [3]:

$$Q_S(\mathbf{r}^N) = \frac{\Lambda_S^{-3S}}{S!} \int d\mathbf{R}^S \exp \left[ -\frac{1}{k_B T} (V_{N,S}(\mathbf{r}^N, \mathbf{R}^S) + V_S(\mathbf{R}^S, t)) \right], \quad (38)$$

and  $\Lambda_S$  is the de-Broglie wavelength for the solvent particles. For the equilibrium fluid  $\Phi_N(\mathbf{r}^N)$  can, in principle, be calculated. In general

$$\Phi_N(\mathbf{r}^N) = \tilde{V} \phi_0 + \sum_{i=1}^N \phi_1(\mathbf{r}_i) + \frac{1}{2} \sum_{j \neq i} \sum_{i=1}^N \phi_2(\mathbf{r}_i, \mathbf{r}_j) + \frac{1}{6} \sum_{k \neq j \neq i} \sum_{j \neq i} \sum_{i=1}^N \phi_3(\mathbf{r}_i, \mathbf{r}_j, \mathbf{r}_k) + \dots, \quad (39)$$

where  $\tilde{V}$  is the volume of the system,  $\phi_0$  is a zero-body potential [3],  $\phi_1(\mathbf{r}_i)$  is the solvent mediated one-body potential (for example with the fluid container walls),  $\phi_2(\mathbf{r}_i, \mathbf{r}_j)$  is a two body pair potential,  $\phi_3(\mathbf{r}_i, \mathbf{r}_j, \mathbf{r}_k)$  is a three body potential, and so on. These potentials are generally density dependent. We shall assume that the non-equilibrium solvent mediated potential is the same as the equilibrium solvent mediated potential (39). This approximation should be reliable on time scales  $\gg \tau_s$ , since on these time scales the solvent particles are effectively at equilibrium. Thus the leading order terms in a Taylor expansion of the force term in Eq. (36) can be expressed as:

$$\left( \frac{\partial f^{(N)}}{\partial t} \right)_{\text{solvent}} \simeq \sum_{i=1}^N \frac{\partial}{\partial \mathbf{p}_i} \cdot \left( (\gamma \mathbf{p}_i - \mathbf{x}_i) f^{(N)} + \theta \frac{\partial f^{(N)}}{\partial \mathbf{p}_i} + \dots \right), \quad (40)$$

where  $\theta$  is a mobility coefficient, which, in principle, is a function of the colloidal phase space coordinates. However, we shall assume  $\gamma$  and  $\theta$  to be constants. If we now substitute Eq. (40) into Eq. (34), retaining only the two leading order terms, then we obtain:

$$\begin{aligned} \frac{\partial f^{(N)}}{\partial t} + \frac{1}{m} \sum_{i=1}^N \mathbf{p}_i \cdot \frac{\partial f^{(N)}}{\partial \mathbf{r}_i} + \sum_{i=1}^N (\mathbf{X}_i + \mathbf{x}_i) \cdot \frac{\partial f^{(N)}}{\partial \mathbf{p}_i} \\ = \gamma \sum_{i=1}^N \frac{\partial}{\partial \mathbf{p}_i} \cdot \mathbf{p}_i f^{(N)} + \theta \sum_{i=1}^N \frac{\partial^2 f^{(N)}}{\partial \mathbf{p}_i^2}. \end{aligned} \quad (41)$$

We recognise this as the Kramers equation – i.e. a generalised Fokker-Planck equation [5]. At this point we can also make the connection between the constants  $\gamma$  and  $\theta$  via the fluctuation dissipation theorem, and we find that  $\theta = m k_B T \gamma$ . In other words, when  $\theta = m k_B T \gamma$ , the *equilibrium* colloid reduced probability distribution function is correctly given by

$$f_0^{(N)} \propto \exp \left[ -\beta \left( \frac{1}{2m} \sum_{i=1}^N |\mathbf{p}_i|^2 + V_N(\mathbf{r}^N) + \Phi_N(\mathbf{r}^N) \right) \right], \quad (42)$$

where  $V_N(\mathbf{r}^N)$ , the term describing the direct interactions between the colloids, is given by Eq. (31) with a time independent external potential.

We now clarify the difference between the potentials  $U_N(\mathbf{r}^N, t)$  in Eq. (8) and  $V_N(\mathbf{r}^N, t)$  in Eq. (31). We see that the total colloid potential  $U_N(\mathbf{r}^N, t)$ , is given by (see Eqs. (31) and (39)):

$$U_N(\mathbf{r}^N, t) = V_N(\mathbf{r}^N, t) + \Phi_N(\mathbf{r}^N). \quad (43)$$

i.e., we see explicitly here that  $U_N(\mathbf{r}^N, t)$  is the sum of the direct colloid interaction potential (31) and the solvent mediated potential (39). In Eq. (8) we can therefore identify the total colloid effective one body potential  $u_{ext}(\mathbf{r}_i) = v_{ext}(\mathbf{r}_i) + \phi_1(\mathbf{r}_i)$ , as the sum of a direct potential and a solvent mediated potential. Similarly, the total colloid effective pair potential  $u_2(\mathbf{r}_i, \mathbf{r}_j) = v_2(\mathbf{r}_i, \mathbf{r}_j) + \phi_2(\mathbf{r}_i, \mathbf{r}_j)$ , the total colloid effective three body potential  $u_3(\mathbf{r}_i, \mathbf{r}_j, \mathbf{r}_k) = v_3(\mathbf{r}_i, \mathbf{r}_j, \mathbf{r}_k) + \phi_3(\mathbf{r}_i, \mathbf{r}_j, \mathbf{r}_k)$ , and the higher body effective potentials are a sum of a direct contribution and a solvent mediated contribution.

The Kramers equation (41) can also be obtained as the (generalised) Fokker-Planck equation for the time evolution of the probability density function for  $N$  colloid particles with the following *stochastic* equations of motion [5]:

$$\begin{aligned} \frac{d\mathbf{r}_i}{dt} &= \frac{\mathbf{p}_i}{m}, \\ \frac{d\mathbf{p}_i}{dt} &= -\gamma\mathbf{p}_i - \frac{\partial}{\partial\mathbf{r}_i}(V_N(\mathbf{r}^N, t) + \Phi_N(\mathbf{r}^N)) + \mathbf{G}_i(t), \end{aligned} \quad (44)$$

where  $\mathbf{G}_i(t) = (\xi_i^x(t), \xi_i^y(t), \xi_i^z(t))$  is a white noise term with correlations given by Eq. (10). In a stochastic treatment of the colloidal fluid one considers the above equations of motion, (44), solely for the colloids and one incorporates the effect of the solvent via the stochastic noise term, the friction coefficient  $\gamma$  and the solvent mediated potential  $\Phi_N(\mathbf{r}^N)$ . In the treatment above, we arrived at the Kramers equation (41) by approximating the Liouville equation for the full system of solvent and colloid particles.

In deriving the Kramers equation (41) it is clear that we made a very large reduction in number of degrees of freedom in the description of the fluid, since we have integrated over the solvent degrees of freedom. However, there are still  $6N$  degrees of freedom in (41) and further reductions are required. We now focus on the colloid probability density function

$$P^{(N)}(\mathbf{r}^N, t) = \int d\mathbf{p}^N f^{(N)}(\mathbf{r}^N, \mathbf{p}^N, t). \quad (45)$$

In order to obtain an equation for the time evolution of  $P^{(N)}(\mathbf{r}^N, t)$  we have to make further approximations. The following is a generalisation of the ‘‘quick and dirty’’ approach in Ref. [2] (see also Refs. [5, 39]). On integrating with respect to the colloid momentum degrees of freedom in Eq. (41), we obtain the following continuity equation:

$$\frac{\partial P^{(N)}}{\partial t} + \sum_{i=1}^N \frac{\partial}{\partial\mathbf{r}_i} \cdot \mathbf{J}_i = 0, \quad (46)$$

where the current

$$\mathbf{J}_i \equiv \int d\mathbf{p}^N \frac{1}{m} \mathbf{p}_i f^{(N)}(\mathbf{r}^N, \mathbf{p}^N, t), \quad (47)$$

and we have used the fact that the integrals  $\int d\mathbf{p}_i(\partial f^{(N)}/\partial \mathbf{p}_i)$ ,  $\int d\mathbf{p}_i(\partial^2 f^{(N)}/\partial \mathbf{p}_i^2)$  and  $\int d\mathbf{p}_i(\partial(\mathbf{p}_i f^{(N)})/\partial \mathbf{p}_i)$  are all equal to zero.

Also, if we multiply Eq. (41) through by  $\mathbf{p}_k/m$ , the velocity of the  $k^{\text{th}}$  colloid, and then integrate over all the colloid momentum degrees of freedom, we obtain:

$$\begin{aligned} \frac{\partial \mathbf{J}_k}{\partial t} + \sum_{i=1}^N \int d\mathbf{p}^N \frac{\mathbf{p}_k}{m} \left( \frac{\mathbf{p}_i}{m} \cdot \frac{\partial f^{(N)}}{\partial \mathbf{r}_i} \right) + \sum_{i=1}^N \int d\mathbf{p}^N \frac{\mathbf{p}_k}{m} \left( (\mathbf{X}_i + \mathbf{x}_i) \cdot \frac{\partial f^{(N)}}{\partial \mathbf{p}_i} \right) \\ = \gamma \sum_{i=1}^N \int d\mathbf{p}^N \frac{\mathbf{p}_k}{m} \frac{\partial}{\partial \mathbf{p}_i} \cdot \mathbf{p}_i f^{(N)} - \gamma m k_B T \sum_{i=1}^N \int d\mathbf{p}^N \frac{\mathbf{p}_k}{m} \frac{\partial^2 f^{(N)}}{\partial \mathbf{p}_i^2}. \end{aligned} \quad (48)$$

If we now make a ‘local momentum equilibrium’ approximation [2], which sets terms such as  $\int d\mathbf{p}^N p_{i,a} p_{j,b} f^{(N)} = m k_B T P^{(N)} \delta_{i,j} \delta_{a,b}$ , where  $p_{i,a}$  is the  $a$ -component ( $a, b = x, y, z$ ) of the momentum of the  $i^{\text{th}}$  particle, then we find that Eq. (48) reduces to

$$\frac{\partial \mathbf{J}_k}{\partial t} + \frac{k_B T}{m} \frac{\partial P^{(N)}}{\partial \mathbf{r}_k} - \frac{1}{m} (\mathbf{X}_k + \mathbf{x}_k) P^{(N)} = -\gamma \mathbf{J}_k. \quad (49)$$

If the friction constant  $\gamma$  is sufficiently large then we can neglect the first term in (49), as it will be negligible compared to the friction term  $-\gamma \mathbf{J}_k$ , on the Brownian time scales  $\tau_B$ , and we obtain:

$$\mathbf{J}_k \simeq -\Gamma k_B T \frac{\partial P^{(N)}}{\partial \mathbf{r}_k} - \Gamma \frac{\partial U_N}{\partial \mathbf{r}_k} P^{(N)}, \quad (50)$$

where  $\Gamma = 1/m\gamma$ . Substituting (50) into Eq. (46), we obtain the Smoluchowski equation (11).

The Smoluchowski equation is generally presented from the stochastic viewpoint, starting from the Langevin equations of motion (9). However, as shown above, one can argue for its use as an approximation to the exact Liouville equations for the time evolution of the probability density function for colloidal fluids. The above derivation demonstrates the physical conditions under which the time evolution of the probability density function of a fluid of colloidal particles is described by the Smoluchowski equation. By going to the Smoluchowski equation (with an effective potentials between the colloids), the description of the fluid is reduced to one based on only the position coordinates of the colloids, rather than the full set of phase space coordinates for the colloid and solvent particles, which is, of course, a significant simplification.

## 5. Discussion and conclusions

In Sec. 2 we introduced the DDFT of Marconi and Tarazona [6, 7] for colloidal fluids, following a recent derivation in Ref. [9] of the DDFT starting from the Smoluchowski equation. We emphasise that this is an approximate theory. In Sec. 3 we applied the DDFT to the specific case of a binary fluid of GCM particles confined in a spherical cavity of variable size. We find that the DDFT is able to describe accurately the time evolution of the highly structured fluid one-body density profiles. We find a variety of collective dynamic processes that are accounted for by the DDFT. For example, the



case in Fig. 5, where we see a particle concentration ‘wave’ travelling through the fluid into the centre of the cavity that allows the fluid to equilibrate into the phase-separated configuration slightly faster than one would expect, bearing in mind the results displayed in Fig. 4, which showed that the fluid-fluid interface persists for a long time after the cavity radius  $\mathcal{R}$  is increased. Such phenomena are very difficult to simulate because of the large number of particles involved. It is in situations such as these where the DDFT should provide a useful tool to analyse the fluid dynamics.

Our strategy is to first consider cases of only a few hundred particles where BD simulations can be used to assess the accuracy of the DDFT results. In these test cases with fewer particles, where the fluid exhibits a limited degree of phase separation and wetting behaviour, we find excellent agreement between the DDFT and the BD simulation results (see for example Figs. 1 and 2). This gives us confidence to trust the reliability of the DDFT when applied to cases with many more particles, where comparison with simulation becomes computationally too expensive. We predict that were one to perform a BD simulation for (say) the cases presented in Figs. 4 and 5, one would find just as good agreement between the DDFT results and BD simulation results. In fact, one should argue that since the total fluid densities are higher in these situations, and the fact that the RPA functional (26) becomes more accurate at higher densities [3, 21], the results from the DDFT should be even more reliable in these cases.

In Sec. 4, we derive the Smoluchowski equation, starting from the exact Liouville equations by making a series of approximations in order to go from a description of the fluid in terms of the full set of colloid and solvent phase space coordinates to a (far more manageable) description solely in terms of the colloid position coordinates (the Smoluchowski equation (11)). Such integration over degrees of freedom is a process that is required in order to render a practical statistical description of any condensed matter system. We believe our derivation is useful because it highlights some of the approximations involved in the Smoluchowski equation for colloids and therefore also in the DDFT and thus sheds light on the status of the DDFT.

The Smoluchowski equation is usually presented from the stochastic viewpoint, since it is the Fokker-Planck equation for the Langevin equations (9). This connection makes it clear that the Smoluchowski equation and thus the DDFT neglect hydrodynamic effects. To include hydrodynamic effects one would have to treat the solvent at a level beyond that taken here, where the effects of the solvent are incorporated in the DDFT via the effective solvent mediated potential between the colloids and in the friction coefficient  $\Gamma^{-1}$ . One can build in hydrodynamic effects in the Smoluchowski equation by replacing  $\Gamma$  with a matrix  $\Gamma_{ij}$ , describing the hydrodynamic coupling between colloids  $i$  and  $j$  [9, 40, 41]. However, this makes the reduction of the Smoluchowski equation to a DDFT much less straightforward.

We conclude that the DDFT, Eq. (20), should provide a good theory for the dynamics of the one body density of a colloidal fluid, even when there is phase separation and wetting of interfaces, provided that i) the friction constant characterising the solvent,  $\Gamma^{-1}$ , is large enough and ii) there exists an accurate approximation for

the excess Helmholtz free energy functional  $\mathcal{F}_{ex}[\rho]$ . Many colloidal fluids can be accurately modelled as effective hard-sphere fluids and therefore we expect that the DDFT combined with fundamental measure free energy functionals [42, 43] for hard spheres to provide a reliable theory for the dynamics of the one body density profile of a (hard-sphere) colloidal fluid.

## Acknowledgments

I am grateful to Christos Likos and Bob Evans for useful discussions and a critical reading of the manuscript. I am also grateful to Christos Likos for providing a static BD simulation code. I acknowledge the support of EPSRC under grant number GR/S28631/01.

## References

- [1] See for example Molloy J E and Padgett M J 2002 *Contemporary Phys.* **43** 241 and references therein
- [2] Barrat J-L and Hansen J-P 2003 *Basic Concepts for Simple Liquids*, Cambridge University Press, Cambridge
- [3] Likos C N 2001 *Phys. Rep.* **348** 267
- [4] Roth R, Evans R and Dietrich S 2000 *Phys. Rev. E* **62** 5360
- [5] Risken H 1984 *The Fokker-Planck Equation*, Springer, Berlin
- [6] Marini Bettolo Marconi U and Tarazona P 1999 *J. Chem. Phys.* **110** 8032
- [7] Marini Bettolo Marconi U and Tarazona P 2000 *J. Phys.: Condens. Matter* **12** A413
- [8] Evans R 1979 *Adv. Phys.* **28** 143
- [9] Archer A J and Evans R 2004 *J. Chem. Phys.* **121** 4246
- [10] Archer A J and Rauscher M 2004 *J. Phys. A: Math. Gen.* **37** 9325
- [11] Dzubiella J and Likos C N 2003 *J. Phys.: Condens. Matter* **15** L147
- [12] Dautenhahn J and Hall C K 1994 *Macromolecules* **27** 5399
- [13] Louis A A, Bolhuis P G, Hansen J-P and Meijer E J 2000 *Phys. Rev. Lett.* **85** 2522
- [14] Bolhuis P G, Louis A A, Hansen J-P, and Meijer E J 2001 *J. Chem. Phys.* **114** 4296
- [15] Louis A A, Bolhuis P G, Finken R, Krakoviack V, Meijer E J and Hansen J-P 2002 *Physica A* **306** 251
- [16] Bolhuis P G and Louis A A 2002 *Macromolecules* **35** 1860
- [17] Likos C N, Rosenfeldt S, Dingenouts N, Ballauff M, Lindner P, Werner N, and Vögtle F 2002 *J. Chem. Phys.* **117** 1869
- [18] Likos C N, Schmidt M, Löwen H, Ballauff M, Pötschke D, and Lindner P 2001 *Macromolecules* **34** 2914
- [19] Lang A, Likos C N, Watzlawek M and Löwen H, *J. Phys.: Condens. Matter* **12** 5087
- [20] Louis A A, Bolhuis P G and Hansen J-P 2000 *Phys. Rev. E* **62** 7961
- [21] Archer A J and Evans R 2001 *Phys. Rev. E* **64** 041501
- [22] Archer A J and Evans R 2002 *J. Phys.: Cond. Matter* **14** 1131
- [23] Archer A J, Likos C N and Evans R 2004 *J. Phys.: Cond. Matter* **16** L297
- [24] Patrykiewicz A, Pizio O and Sokolowski S 2004 *Mol. Phys.* **102** 801
- [25] Penna F and Tarazona P 2003 *J. Chem. Phys.* **68** 1766
- [26] Penna F, Dzubiella J and Tarazona P 2003 *Phys. Rev. E* **68** 061407
- [27] Rex M, Löwen H, and Likos C N 2004 submitted
- [28] Evans R 1992, in *Fundamentals of Inhomogeneous Fluids*, ed. Henderson D, Dekker, New York, ch. 3
- [29] Hansen J-P and McDonald I R 1986 *Theory of Simple Liquids*, Academic, London, 2nd ed.

- [30] Dhont J K G 1996 *An Introduction to Dynamics of Colloids*, Elsevier, Amsterdam
- [31] Dhont J K G 1996 *J. Chem. Phys.* **105** 5112
- [32] Rowlinson J S and Widom B 1982 *Molecular Theory of Capillarity*, Oxford University Press, Oxford
- [33] Archer A J, Evans R and Roth R 2002 *Europhys. Lett.* **59** 526
- [34] Archer A J and Evans R 2003 *J. Chem. Phys.* **118** 9726
- [35] Archer A J, Evans R, Roth R and Oettel M 2005 *J. Chem. Phys.* accepted, *cond-mat/0411557*
- [36] Allen M P and Tildesley T J 1989 *Computer Simulation of Liquids*, Oxford: Clarendon
- [37] Résibois P 1968 *Electrolyte Theory*, Harper and Row, New York
- [38] Résibois P and DeLeener M 1977 *Classical Kinetic Theory of Fluids*, John Wiley, New York
- [39] Bocquet L 1997 *Am. J. Phys.* **65** 140
- [40] Pusey P N and Tough R J A 1985, in *Dynamic Light Scattering*, ed. Pecora R, Plenum Press, New York
- [41] Verberg R, de Schepper I M and Cohen E G D 2000 *Phys. Rev. E* **61** 2967
- [42] Rosenfeld Y 1989 *Phys. Rev. Lett.* **63** 980
- [43] Roth R, Evans R, Lang A and Kahl G 2002 *J. Phys. Cond. Matter* **14** 12063